Fall 2017

COORDINATION OF LEADER-FOLLOWER MULTI-AGENT SYSTEM WITH TIME-VARYING OBJECTIVE FUNCTION

Zalan Mark Fabian
University of New Hampshire, Durham

COORDINATION OF LEADER-FOLLOWER MULTI-AGENT SYSTEM WITH TIME-VARYING OBJECTIVE FUNCTION

by

Zalan M. Fabian
BSc. in Electrical Engineering, Budapest University of Technology, 2014

THESIS

Submitted to the University of New Hampshire
in Partial Fulfillment of
the Requirements for the Degree of

Master of Science
in
Electrical Engineering

September, 2017

THESIS COMMITTEE PAGE

This thesis has been examined and approved in partial fulfillment of the requirements for the degree of Master of Science in Electrical Engineering by:

- Thesis Director, Se Young Yoon, Assistant Professor at the Department of Electrical and Computer Engineering
- Andrew L. Kun, Associate Professor at the Department of Electrical and Computer Engineering
- May-Win Thein, Associate Professor at the Department of Mechanical Engineering

On May 19, 2017

Original approval signatures are on file with the University of New Hampshire Graduate School.

"...technology is - not an exploitation of nature, but a fusion of nature and the human spirit into a new kind of creation that transcends both."

Robert M. Pirsig

ABSTRACT

COORDINATION OF LEADER-FOLLOWER MULTI-AGENT SYSTEM WITH TIME-VARYING OBJECTIVE FUNCTION

by

Zalan M. Fabian

University of New Hampshire, September, 2017

This thesis aims to introduce a new framework for the distributed control of multi-agent systems with adjustable swarm control objectives. Our goal is twofold: 1) to provide an overview to how time-varying objectives in the control of autonomous systems may be applied to the distributed control of multi-agent systems with variable autonomy level, and 2) to introduce a framework to incorporate the proposed concept to fundamental swarm behaviors such as aggregation and leader tracking. Leader-follower multi-agent systems are considered in this study, and a general form of time-dependent artificial potential function is proposed to describe the varying objectives of the system in the case of complete information exchange. Using Lyapunov methods, the stability and boundedness of the agents' trajectories under single order and higher order dynamics are analyzed. Illustrative numerical simulations are presented to demonstrate the validity of our results. Then, we extend these results for multi-agent systems with limited information exchange and switching communication topology. The first steps of the realization of an experimental framework have been made with the ultimate goal of verifying the simulation results in practice.

Acknowledgements

Firstly, I would like to thank my advisor Professor Se Young Yoon of the Electrical and Computer Engineering Department at the University of New Hampshire. It was him who's ambitious vision of this project always steered me in the right direction from the very beginning to the final state. Professor Yoon was consistently available whenever I needed guidance and provided invaluable advice. He supported me not only as his student but also as a human being.

I would also like to thank Jim Abare of the Electrical and Computer Engineering Department's Engineering Technician at the University of New Hampshire. Jim designed and built the protective cage for our experiments and he was always available when I needed technical help in the laboratory.

I would also like to acknowledge my labmates Himadri Basu and Khalid M. Arthur of the Electrical and Computer Engineering Department at the University of New Hampshire for providing vaulable comments on this thesis. It was a pleasure coming to the lab every day and working with such great people.

Last but not least, I would like to express my gratitude to my family for providing me with unfailing support and encouragement throughout these years when I needed it the most. This accomplishment could not have been possible without them.

Contents

List of Figures

Chapter 1

Introduction

1.1 Introduction

Swarming is a commonly observed behavior in nature, and it grants certain species significant advantages to their survival. Examples include schools of fish, packs of wolves, colonies of ants or flocks of birds. This collective behavior was examined extensively by experts of interdisciplinary fields [3–5], and it was successfully mimicked in optimization algorithms [6–8] and distributed control problems, such as consensus [9], flocking [10], formation control [11] and coverage control of sensor networks [12]. The term *swarm* in engineering may refer to a group of vehicles, robots, other agents with individual dynamics, but with some coupled behavior that binds them in working towards a common goal.

By analyzing the swarming phenomenon occurring in nature, the associated control problems can be divided into the following categories. *Aggregation* [13] is one of the most fundamental behaviors, and it refers to the process of swarm members grouping into a cluster. In other words, looking at the multi-agent system as time approaches infinity, the agent states are within a bounded region. In some cases the agents may need to approach a moving target and stay in its vicinity, which is usually referred to as *swarm tracking* [14] or *hunting* [15]. *Social foraging* on the other hand is a more complex behavior, which is illustrated in [16] by considering simple life forms, such as bacteria searching for nutrients. The swarm members are attracted to locations with high nutrient concentration, and repelled by spots of poisonous substances. The attractive or repulsive forces applied by the environment may be modeled by a resource profile function.

There are numerous applications with strong arguments for the use of autonomous robotic swarms, and they include operations in reconnaissance [17], demining [18], exploration [19], and

resource mining [20]. Moreover, a growing interest can be observed in the commercial sector as well, mainly for applications in warehousing or product delivery [21, 22]. The properties which make swarms more desirable than single robots include robustness, flexibility, multi-tasking potential and cost-effectiveness. Furthermore, the structure of an individual agent, both by means of hardware and software, can be significantly simpler than a single complex intelligent robot, rendering it to be easily testable and less prone to errors.

Although fully autonomous robotic swarms are capable of performing complex tasks, the supervision by a human operator still plays an essential role in practical applications. The interaction of the human operator with an autonomous swarm may be captured by a leader-follower multi-agent system framework, where the human leader oversees the follower agents and coordinates their motion to achieve a global goal. Walker *et al.* investigated a robotic swarm maneuvered to goal points by a human operator [23]. Goodrich *et al.* construct a framework of human interaction with bio-inspired robot teams [24]. Flocking algorithms with a virtual leader have been widely explored in the literature. In the work of Meng *et al.* the swarm is divided into a leader group and a follower group and swarm tracking and velocity matching is achieved [25]. Shi *et al.* used a virtual leader as an external reference signal for a group of autonomous agents with point mass dynamics [26]. Gu and Wang proposed a leader-follower algorithm, in which the followers have no information of which agents are part of the leader set [27]. Su *et al.* investigated virtual leaders with varying velocity, generalizing well-known results from the literature [28].

A weakness of the above described human-machine hybrid system is that the performance of the human operator may be unreliable due to unmodeled physiological or psychological factors, such as fatigue, stress, or external distractions. Under optimal conditions, the follower agents may rely on the input from the human operator for guidance in achieving the global goals of the overall system. However, due to the aforementioned factors affecting the human leader, a better solution to the system-level goal may be obtained by increasing the autonomy of the follower agents and granting them more independence to pursue their own local objectives. In other words, dynamically changing autonomy levels may result in a safer and more effective control strategy for the autonomous system, when compared to a system with fixed interaction rules between the human operator and the autonomous subsystems.

The idea of manipulating the autonomy of robotic systems has been gaining ground in recent years, and it is commonly referred to as adjustable, sliding or adaptive autonomy [29–31]. Reference [32] presents an experiment in the control of a robotic system with discrete autonomy modes that ranges from full autonomy to basic teleoperation. The authors of [33] propose a decision-theoretic approach where the autonomy level is closely related to the attention level of

a supervision unit. A Mixed Markov Decision Process is used to model the system behavior, in which the states represent both the system state and the discrete level of attention. In [34] and [30] the focus is on introducing transfer-of-control strategies, and these strategies are applied to real-world examples of multi-agent systems. The application of adjustable autonomy for future space missions is investigated in [35].

The adaptive autonomy level of a swarm may also be considered to be a continuous time-dependent parameter of the multi-agent system. This parameter can be provided to the follower agents of the swarm by a "global planner", with some underlying dynamics unknown to the agents. In practice, this might mean that the condition of the human operator is monitored (see for example [36]), and the optimal autonomy level is determined and broadcast to the swarm. Alternatively, one can consider the "autonomy" parameter as a measure of leader reliability based on its past actions perceived by the swarm. In this approach the agents observe the leader's actions, and decide on the level of autonomy either individually or collectively through consensus algorithms.

Motivated by the aforementioned ideas, the objective of this thesis work is to provide a framework of time-varying objective functions in the context of multi-agent leader-follower systems and to analyze certain fundamental swarm behaviors such as leader tracking or aggregation in the proposed framework. The problem is investigated under different agent dynamics and communication topologies. To our knowledge, continuous time-varying objective functions for leader-follower distributed systems has not yet been investigated in the literature and therefore it is the main contribution of this work. Experimental validation of the proposed methods is also a significant aspect of the project which cannot be overlooked. Therefore, the first steps of the realization of an experimental framework has been implemented as part of this work.

1.2 Preliminaries

In a swarm with N agents, the dynamics of the i^{th} agent in the swarm has the general form

$$\dot{x}_i = f_i(x_i, u_i),$$

where $x_i \in \mathbb{R}^n$ represents the state of agent i and $u_i \in \mathbb{R}^m$ is the control input to agent i. The state may be position, orientation or any other measure we select as a state depending on the particular application.

If the agent dynamics are the same for every agent, that is if

$$f_i(x', u') = f_j(x', u')$$

for every i, j pairs, where $i, j \in 1, 2, .., N$ and for every $x' \in \mathbb{R}^n$ and $u' \in \mathbb{R}^m$, then the swarm is *homogeneous*. If a swarm is not homogeneous, it is said to be *heterogeneous*.

The order of a dynamic system is the order of the differential equation governing it, that is the order of the highest derivative present with respect to time in the dynamics. A first-order system is also called a *single-integrator* system, whereas a second-order system is referred to as *double-integrator*. Systems with order above two are usually said to have higher-order dynamics.

A leader-follower multi-agent system is a heterogeneous system, where a subset of the agents constitute the leader group, while the other agents are followers. The leaders are distinguished in a sense that they either have access to a broader set of information, which they broadcast to the followers, or the leaders' state serve as tracking objective for followers. In practice this might mean that leaders are responsible for guiding the swarm or maintaining the formation due to their ability to access more sensor data or external information than the followers.

Agents share information about their state through a communication network, and the topology of this network is described as a graph structure, therefore it is necessary to introduce some concepts and results from graph theory (mostly from an algebraic graph theory point of view).

A *directed graph*, or *digraph* $G(V, E)$ consists of a vertex set V and an edge set E, where an arc, or directed edge is an ordered pair of distinct vertices. If an edge exists between two distinct vertices, they are called adjacent. A *path* in a directed graph $G(V, E)$ is a sequence $u_0, ..., u_r$ of distinct vertices such that (u_{i-1}, u_i) is an arc of G for $i = 1, .., r$. A digraph is said to be *strongly connected* if any two vertices can be joined by a path. If the edge set consists of unordered pairs of distinct vertices, the graph is called *undirected*. A *subgraph* $F(V', E')$ of a graph $G(V, E)$ is such that $V' \subseteq V$, and $E' \subseteq E$. If $V' = V$, we call F a *spanning subgraph*. A graph is called complete if every pair of vertices are adjacent. [37]

A weighted directed graph is a triple (V, E, A). Here (V, E) is a digraph with n vertices and $A = [a_{ij}]$ is its $n \times n$ weighted adjacency matrix with entry $a_{ij} \geq 0$ as the *weight* of the directed edge from vertex i to j (we exclude self-joining edges, i.e. $a_{ii} = 0$). The weight of edge e is denoted as $w(e)$.

A weighted directed graph $G(V, E, A)$ with vertex set V, edge set E, and adjacency matrix $A = [a_{ij}]_{N \times N}$, is called balanced if $\sum_{j=1, j \neq i}^{N} a_{ji} = \sum_{j=1, j \neq i}^{N} a_{ij}$ for any vertex $i \in V$. An $N \times N$ *permutation matrix* is any $N \times N$ matrix which can be obtained by rearranging the rows and/or

columns of the $N \times N$ identity matrix. A square matrix $A \in \mathbb{R}^{N\times N}$ is said to be *reducible* if a permutation matrix P exists such that P^TAP is block upper triangular. If a square matrix is not reducible, it is called *irreducible*. A digraph with adjacency matrix A is strongly connected if and only if A is irreducible.

Lemma 1.1. *[38][39] Let a matrix $W = [w_{ij}] \in \mathbb{R}^{N\times N}$. Suppose that $w_{ij} \geq 0$ for $i \neq j$ and $w_{ii} = -\sum_{j=1,j\neq i}^{N} w_{ij} < 0$ for $i = 1, 2, ..., M$. Then*

1. *$\lambda = 0$ is an eigenvalue of W with a right eigenvector $[1\ 1\ ...\ 1]^T$. The eigenvalues of W have the property $Re(\lambda_i) \leq 0$.*
2. *Let $\xi = [\xi_1\ \xi_2\ ...\ \xi_N]$ be a left eigenvector of W corresponding to the zero eigenvalue; then, there exists at least one ξ such that $\xi_i \geq 0 \quad \forall i = 1, 2, ..., N$, also denoted as $\xi \geq 0$. W is irreducible if and only if there exists one $\xi > 0$. If W is irreducible, then zero is an eigenvalue of W with multiplicity of one.*
3. *If W is irreducible, then $W + W^T$ and $EW + W^TE$ are both irreducible, where $E = diag(\xi_1, \xi_2, ..., \xi_N)$.*
4. *Without loss of generality assume that $\sum_{i=1}^{N} \xi_i = 1$. Then, $\xi = \frac{1}{N}[1\ 1\ ...\ 1]^T$ if and only if $\sum_{j=1,j\neq i}^{N} w_{ji} = \sum_{j=1,j\neq i}^{N} w_{ij}$ holds. Moreover, in this case $W + W^T$ is negative semi-definite.*

Let $L(G) = [l_{ij}]$ denote the *Laplacian matrix* of weighted graph $G(V, E, A)$ on n vertices, where

$$l_{ij} = \begin{cases} -a_{ij} & \text{if} \quad i \neq j \\ \sum_{j=1,j\neq i}^{N} a_{ij} & \text{if} \quad i = j. \end{cases}$$

Notice, that Lemma 2.2 directly concerns $-L(G)$, therefore the smallest eigenvalue of $L(G)$ is 0, with a multiplicity of 1 if and only if G is connected. Hence, if weighted graph G is connected then the eigenvalues of $L(G)$, also called the *Laplacian eigenvalues*, can be enumerated as $0 = \lambda_1 < Re(\lambda_2) \leq Re(\lambda_3) \leq ... \leq Re(\lambda_N)$. For weighted undirected graphs, all the eigenvalues are real and λ_2 is also known as the *algebraic connectivity*, and has many interesting properties related to graph invariants[40]. The magnitude of λ_2 reflects how well-connected a graph is and therefore has been frequently used to analyze the stability and robustness of multi-agent systems and networks.

Lemma 1.2. *Consider a weighted undirected graph $G(V, E, A)$ with N vertices and algebraic connectivity $\lambda_2(G)$. Denote $w(e)$ the weight of edge $e \in E$.*

1. *Form graph G_1 from G by reducing the weight of edge e to a new value $w_1(e)$, so that $w_1(e) \leq w(e)$. Then $\lambda_2(G_1) \leq \lambda_2(G)$, and equality holds if and only if $w_1(e) = w(e)$ [41].*

2. *Form graph G_2 from G by increasing the weight of edge e to a new value $w_2(e)$, so that $w_2(e) \geq w(e)$. Then $\lambda_2(G_2) \geq \lambda_2(G)$, and equality holds if and only if $w_2(e) = w(e)$ [41].*

3. *Let G_3 be a spanning subgraph of graph G. Then, $\lambda_2(G_3) \leq \lambda_2(G)$ [40].*

4. *Form graph $G_4(V, E', A')$ from G by inserting a new edge e into G, that is $E' = E \cup \{e\}$. Then, the eigenvalues of G and G_4 interlace: $0 = \lambda_1(G) = \lambda_1(G_4) \leq \lambda_2(G) \leq \lambda_2(G_4) \leq \lambda_3(G) \leq ... \leq \lambda_N(G) \leq \lambda_N(G_4)$ [40].*

1.3 Organization

In Chapter 2 a distributed control framework is introduced to incorporate leader-follower multi-agent systems with time-varying objectives, given that every follower has access to the state of every other agent and the leader (completely connected communication topology). In Chapter 3 the results are extended and the complete information exchange assumption is relaxed to balanced communication topology. Moreover it is shown how the proposed framework can tackle switching topologies and collision avoidance problems. Chapter 4 demonstrates the first steps towards the experimental validation of the proposed distributed control scheme. Chapter 5 discusses future directions and concludes the current study.

This introduction and the following chapter demonstrates the results published in [42] by Z. Fabian and S.Y. Yoon with extension to agents with uncertain higher order dynamics.

Chapter 2

Coordinated control under complete communication graph

2.1 Introduction

In this chapter, we study the coordinated control of leader-follower multi-agent systems with time-dependent objectives and completely connected communication topology, and we develop a framework to incorporate the varying autonomy level of follower agents to the swarm control problem. Complete connectedness implies that the state of any agent is available to every other agents at any time t. In particular, the swarm aggregation and leader tracking problem is studied, where the time-dependent objectives of the swarm are introduced as time-varying parameters of the artificial potential functions. These time-varying parameters of the potential function govern the virtual interaction forces between the follower agents and the leader, and they can be used to relax or tighten the formation of the agents around the leader. For the considered control problem, we employ Lyapunov methods to demonstrate the stability and boundeness of the the agents' trajectories. This is initially proven for single integrator agents, and then expanded to agents with higher order dynamics. For the follower agents, a time-bound is also provided for their convergence to the final formation.

The organization of the chapter is as follows. Section 2.2 defines the framework involving the applied artificial potential functions. Section 2.3 analyzes the aggregation problem with single-integrator agents and a leader, and an ultimate bound for the swarm size is derived. These results are then extended to uncertain higher order agent dynamics in Section 2.4. Illustrative

simulation results are included in Section 2.5 to further explain the presented ideas. Finally, we draw conclusions in Section 2.6.

2.2 Artificial potential functions for adjustable autonomy levels

In order to define our framework, consider a generic swarm involving N agents and a leader. We will denote the state of agent i with the column vector $x_i \in \mathbb{R}^n$ and the state of the leader agent with the column vector $x_{\mathrm{L}} \in \mathbb{R}^n$. The state might represent the location or any other desired parameter of the agent. Let u_i denote the control input to agent i. An artificial potential function $V : \mathbb{R}^{(N+1)n} \mapsto \mathbb{R}$, also referred to as *global potential function*, describes the global objectives of the system by assigning a scalar value to admissible configurations of the agent states.

Assume, that

$$u_i = -\nabla_{x_i} V(x), \tag{2.1}$$

where x is the stacked state vector $x^T = [x_1^T \; x_2^T \; \cdots \; x_N^T \; x_{\mathrm{L}}^T]$. This means that the agents' dynamics are governed by the negative gradient of the underlying artificial potential field evaluated at the respective agent's current states.

In our framework, $V(x)$ is the superposition of local potential functions

$$V = \frac{1}{2}\sum_{i=1}^{N} V_i = \frac{1}{2}\sum_{i=1}^{N}(V_i^{\mathrm{a}} - V_i^{\mathrm{r}}), \tag{2.2}$$

where $V_i^{\mathrm{a}} : \mathbb{R}^+ \mapsto \mathbb{R}$ and $V_i^{\mathrm{r}} : \mathbb{R}^+ \mapsto \mathbb{R}$ represent the attractive and repulsive component of the potential field, respectively. Both V_i^{a} and V_i^{r} are functions of the inter-agent distances. Further assume that, for some $f_{i,j}$, $f_{i,\mathrm{L}} : \mathbb{R}^+ \mapsto \mathbb{R}$, the gradient of the local potential function can be written in the following form:

$$\nabla_{x_i} V_i(x) = \sum_{j=1}^{N} f_{i,j}(\|x_i - x_j\|)(x_i - x_j) + f_{i,\mathrm{L}}(\|x_i - x_{\mathrm{L}}\|)(x_i - x_{\mathrm{L}}). \tag{2.3}$$

One can interpret $f_{i,j}$ as the magnitude of the resulting "force" vector acting between agent i and j (or $f_{i,\mathrm{L}}$ between agent i and the leader L).

Now, from (3.2), (2.2) and (2.3) we have

$$u_i = -\sum_{j=1}^{N} f_{i,j}(\|x_i - x_j\|)(x_i - x_j) - f_{i,\mathrm{L}}(\|x_i - x_\mathrm{L}\|)(x_i - x_\mathrm{L}). \tag{2.4}$$

We may further break down this inter-agent force into attractive and repulsive components:

$$f_{i,j}(\|x_i - x_j\|) = f^{\mathrm{a}}_{i,j}(\|x_i - x_j\|) - f^{\mathrm{r}}_{i,j}(\|x_i - x_j\|), \tag{2.5}$$

and

$$f_{i,\mathrm{L}}(\|x_i - x_\mathrm{L}\|) = f^{\mathrm{a}}_{i,\mathrm{L}}(\|x_i - x_\mathrm{L}\|) - f^{\mathrm{r}}_{i,\mathrm{L}}(\|x_i - x_\mathrm{L}\|). \tag{2.6}$$

Superscript "a" and "r" denote the attractive and repulsive components, respectively. Swarm aggregation is achieved by the interplay of the virtual attractive and repulsive forces resulting from the underlying artificial potential function. Attractive forces dominate on large distances to ensure swarm cohesion, while repulsion forces dominate on short distances to avoid collision. Also, without repulsive forces the whole swarm would collapse into a single point, whereas without attractive forces the swarm would disperse.

To incorporate the aforementioned points into the framework, we introduce the following assumption.

Assumption 1. The inter-agent virtual force functions satisfy $f_{i,j} = f_{j,i}$ for neighboring agents i and j, and unique equilibrium distance $d_e > 0$ exists for all $f_{i,j}$, where $f^{\mathrm{a}}_{i,j}(d_e) = f^{\mathrm{r}}_{i,j}(d_e)$. Moreover, $f^{\mathrm{a}}_{i,j}(d) > f^{\mathrm{r}}_{i,j}(d)$ for any $d > d_e$, and $f^{\mathrm{r}}_{i,j}(d) > f^{\mathrm{a}}_{i,j}(d)$ for any $0 < d < d_e$.

In this chapter, we consider the case where the attractive force increases linearly with the inter-agent distance, whereas the repulsive forces are bounded. To incorporate the adjustable autonomy in our framework, we let the attractive and repulsive forces to be time-varying functions of the inter-agent distance, and with some restrictions as detailed below.

Assumption 2. Let

$$f^{\mathrm{a}}_{i,j}(\|x_i - x_j\|, t) = k^{\mathrm{a}}(t),$$
$$f^{\mathrm{a}}_{i,\mathrm{L}}(\|x_i - x_\mathrm{L}\|, t) = k^{\mathrm{a}}_{\mathrm{L}}(t).$$

There exist $\underline{k}^{\mathrm{a}}, \overline{k}^{\mathrm{a}}, \underline{k}^{\mathrm{a}}_{\mathrm{L}}, \overline{k}^{\mathrm{a}}_{\mathrm{L}} \in \mathbb{R}^+$ such that $\underline{k}^{\mathrm{a}} < k^{\mathrm{a}}(t) < \overline{k}^{\mathrm{a}}$ and $\underline{k}^{\mathrm{a}}_{\mathrm{L}} < k^{\mathrm{a}}_{\mathrm{L}}(t) < \overline{k}^{\mathrm{a}}_{\mathrm{L}}$ for all t. Furthermore, there exist $\overline{F}^{\mathrm{r}}, \overline{F}^{\mathrm{r}}_{\mathrm{L}} \in \mathbb{R}^+$ such that

$$0 < f^{\mathrm{r}}_{i,j}(\|x_i - x_j\|, t)\|x_i - x_j\| < \overline{F}^{\mathrm{r}},$$
$$0 < f^{\mathrm{r}}_{i,\mathrm{L}}(\|x_i - x_\mathrm{L}\|, t)\|x_i - x_\mathrm{L}\| < \overline{F}^{\mathrm{r}}_{\mathrm{L}}.$$

An example for a potential function satisfying these assumptions is

$$V_i(x) = \sum_{j=1}^{N} \left(\frac{k^{\mathrm{a}}(t)}{2} \|x_i - x_j\| + \frac{k_r r}{2} \mathrm{e}^{-\frac{\|x_i - x_j\|^2}{r}} \right) + \frac{k_{\mathrm{L}}^{\mathrm{a}}(t)}{2} \|x_i - x_{\mathrm{L}}\| + \frac{k_{\mathrm{L}}^{\mathrm{r}} r_{\mathrm{L}}}{2} \mathrm{e}^{-\frac{\|x_i - x_{\mathrm{L}}\|^2}{r_{\mathrm{L}}}}. \tag{2.7}$$

The corresponding virtual interaction forces acting on the agents are

$$\begin{aligned} \nabla_{x_i} V_i(x) = &- \sum_{j=1}^{N} \left(k^{\mathrm{a}}(t) - k^{\mathrm{r}} \mathrm{e}^{-\frac{\|x_i - x_j\|^2}{r}} \right) (x_i - x_j) \\ &- \left(k_{\mathrm{L}}^{\mathrm{a}}(t) - k_{\mathrm{L}}^{\mathrm{r}} \mathrm{e}^{-\frac{\|x_i - x_{\mathrm{L}}\|^2}{r_{\mathrm{L}}}} \right) (x_i - x_{\mathrm{L}}). \end{aligned} \tag{2.8}$$

2.3 Aggregation with single-integrator dynamics

In this section we investigate the swarm behavior and stability for a system with single-integrator agent dynamics and an immobile leader. In particular, let

$$\dot{x}_i = u_i, \qquad i = 1, 2, \cdots, N, \tag{2.9}$$

and

$$\dot{x}_{\mathrm{L}} = 0. \tag{2.10}$$

The artificial potential functions introduced in the previous section ensures the aggregation of the follower agents, keeping them in close proximity to each other and forming a cohesive group. In particular, we use the following definition for the aggregation problem.

Definition 2.1. *(Aggregation)* Consider a swarm consisting of N agents, with states $x_i(t) \in \mathbb{R}^n$ for $i = 1, 2, \cdots, N$. Design the corresponding control inputs $u_i(t)$ for all agents $i = 1, 2, \cdots, N$ and $j = 1, 2, \cdots, N$ so that

$$\lim_{t \to \infty} \|x_i(t) - x_j(t)\| \leq 2\epsilon$$

for some $\epsilon > 0$.

Our goal is to determine the expected ultimate swarm size of the multi-agent system when the forces of attraction and repulsion are varying within the predefined limits in Assumptions 1 and 2. Define the swarm centroid as

$$\overline{x} = \frac{1}{N} \sum_{i=1}^{N} x_i. \tag{2.11}$$

Excluding the leader from the system, the swarm centroid is stationary due to the symmetry of the interaction forces (see proof in [43]). However, taking the leader into consideration, the asymmetry of the interaction forces results in the motion of swarm centroid. The asymmetry originates in the fact that the leader is not affected by the inter-agent interaction forces. Our intuition suggests that the centroid movement is governed by the leader attraction and repulsion imposed to the follower agents.

Lemma 2.2. *Consider a swarm consisting of N agents with dynamics (2.9), a leader agent with dynamics (2.10) and control input (2.4), where Assumption 1 is satisfied. Then, the swarm centroid dynamics are governed exclusively by the leader interaction forces as follows:*

$$\dot{\bar{x}} = -\frac{1}{N}\sum_{i=1}^{N} f_{i,L}(\|x_i - x_L\|)(x_i - x_L).$$

Proof. Substituting the agent dynamics and control law from (2.4) into the derivative of the swarm centroid we have

$$\dot{\bar{x}} = \frac{1}{N}\sum_{i=1}^{N}\dot{x_i} = -\frac{1}{N}\sum_{i=1}^{N}\sum_{j=1}^{N} f_{i,j}(\|x_i - x_j\|)(x_i - x_j) - \frac{1}{N}\sum_{i=1}^{N} f_{i,\mathrm{L}}(\|x_i - x_\mathrm{L}\|)(x_i - x_\mathrm{L}). \quad (2.12)$$

By reorganizing the summation limits and applying the fact that $f_{i,j}(\|x_i - x_j\|) = f_{j,i}(\|x_j - x_i\|)$, we can state that

$$\frac{1}{N}\sum_{i=1}^{N}\sum_{j=1}^{N} f_{i,j}(\|x_i - x_j\|)(x_i - x_j) = \frac{1}{N}\sum_{i=1}^{N-1}\sum_{j=i}^{N}(f_{i,j}(\|x_i - x_j\|)(x_i - x_j) + f_{j,i}(\|x_j - x_i\|)(x_j - x_i)) = 0.$$

Hence the first term in (2.12) is 0, which completes the proof. □

As we see, the system behavior can be described as follows: the follower agents aggregate around their centroid, which is drawn to the leader at the same time. To determine the ultimate swarm size, the first step is to investigate how close the swarm centroid can approach the leader. The reason why a non-zero ultimate centroid-leader distance might exist is that the leader attractive force might not be strong enough to "break apart" the cohesive group of aggregated follower agents.

Lemma 2.3. *Consider a swarm consisting of N agents with dynamics (2.9), a leader agent with dynamics (2.10) and control input (2.4), where Assumptions 1 and 2 are satisfied. Let*

$\tilde{e} = \overline{x} - x_L$ denote the vector from the leader to the swarm centroid. As $t \to \infty$ the swarm centroid asymptotically approaches the hyperball around the leader such that

$$\|\tilde{e}\| < \frac{\overline{F}_L^r}{\underline{k}_L^a}. \tag{2.13}$$

Moreover, the swarm centroid enters any hyperball around the leader with radius

$$\|\tilde{e}\| = \frac{\overline{F}_L^r}{\underline{k}_L^a(1-\delta)} := K_\delta,$$

$0 < \delta < 1$, *in finite time bounded by*

$$T_\delta = -\frac{1}{2\underline{k}_L^a \delta} \ln\left[\frac{K_\delta^2}{\|\tilde{e}(0)\|^2}\right].$$

Proof. Consider the following Lyapunov function candidate:

$$W(x) = \frac{1}{2}\tilde{e}^T\tilde{e}.$$

Taking its time derivative along the agent trajectories yields

$$\dot{W} = \dot{\tilde{e}}^T\tilde{e} = (\dot{\overline{x}} - \dot{x_{\mathrm{L}}})^T(\overline{x} - x_{\mathrm{L}}) = \dot{\overline{x}}^T\tilde{e}.$$

Applying Lemma 2.2 we have

$$\dot{W} = -\frac{1}{N}\sum_{i=1}^{N} f_{i,\mathrm{L}}(\|x_i - x_{\mathrm{L}}\|)(x_i - x_{\mathrm{L}})^T\tilde{e}.$$

Substituting the attraction and repulsion terms from Assumption 2 yields

$$\dot{W} = -\frac{1}{N}\sum_{i=1}^{N} k_{\mathrm{L}}^{\mathrm{a}}(t)(x_i - x_{\mathrm{L}})^T\tilde{e} + \frac{1}{N}\sum_{i=1}^{N} f_{i,\mathrm{L}}^{\mathrm{r}}(x_i - x_{\mathrm{L}})^T\tilde{e}.$$

Notice, that

$$\sum_{i=1}^{N}(x_i - x_{\mathrm{L}}) = N\overline{x} - Nx_{\mathrm{L}} = N\tilde{e}.$$

Hence, we have

$$\dot{W} = -k_{\mathrm{L}}^{\mathrm{a}}(t)\|\tilde{e}\|^2 + \frac{1}{N}\sum_{i=1}^{N} f_{i,\mathrm{L}}^{\mathrm{r}}(x_i - x_{\mathrm{L}})^T\tilde{e}.$$

Applying the upper bound on the repulsion terms from Assumption 2 and the Cauchy-Schwarz inequality yields

$$\dot{W} \leq -k_{\mathrm{L}}^{\mathrm{a}}(t)\|\tilde{e}\|^2 + \overline{F}_{\mathrm{L}}^{\mathrm{r}}\|\tilde{e}\| = \|\tilde{e}\|\left(-k_{\mathrm{L}}^{\mathrm{a}}(t)\|\tilde{e}\| + \overline{F}_{\mathrm{L}}^{\mathrm{r}}\right). \tag{2.14}$$

Consequently, if $\frac{\overline{F}_{\mathrm{L}}^{\mathrm{r}}}{k_{\mathrm{L}}^{\mathrm{a}}(t)} < \|\tilde{e}\|$, then $\dot{W} < 0$. In the region where the previous inequality holds, the Lyapunov-function must decrease, which means that the leader-centroid distance is decreasing. Since for all t we have

$$\frac{\overline{F}_{\mathrm{L}}^{\mathrm{r}}}{k_{\mathrm{L}}^{\mathrm{a}}(t)} \leq \frac{\overline{F}_{\mathrm{L}}^{\mathrm{r}}}{\underline{k}_{\mathrm{L}}^{\mathrm{a}}}$$

the leader-centroid distance must decrease if

$$\frac{\overline{F}_{\mathrm{L}}^{\mathrm{r}}}{\underline{k}_{\mathrm{L}}^{\mathrm{a}}} < \|\tilde{e}\|,$$

therefore as $t \to \infty$,

$$\frac{\overline{F}_{\mathrm{L}}^{\mathrm{r}}}{\underline{k}_{\mathrm{L}}^{\mathrm{a}}} \geq \|\tilde{e}\|,$$

which serves as an upper bound for the leader-centroid ultimate distance.

From (2.14) one may notice that if we let

$$\|\tilde{e}\| \geq \frac{\overline{F}_{\mathrm{L}}^{\mathrm{r}}}{\underline{k}_{\mathrm{L}}^{\mathrm{a}}(1-\delta)},$$

then

$$\dot{W} \leq -\underline{k}_{\mathrm{L}}^{\mathrm{a}}\delta\|\tilde{e}\|^2.$$

Due to the fact that we defined our Lyapunov function as $W = \frac{1}{2}\|\tilde{e}\|^2$, and by applying the comparison principle we conclude that

$$W(t) \leq W(0)\,\mathrm{e}^{-2\delta\underline{k}_{\mathrm{L}}^{\mathrm{a}}t}.$$

Thus the maximum time T_δ necessary for the swarm centroid to approach the leader in distance $\|\tilde{e}\| = K_\delta$ is obtained from the inequality above and by substituting $W = \frac{1}{2}K_\delta^2$. In particular, solving for the aforementioned conditions yields

$$T_\delta = \frac{1}{-2\underline{k}_{\mathrm{L}}^{\mathrm{a}}\delta}\ln\left[\frac{1}{2W(0)}K_\delta^2\right],$$

which completes the proof. □

Since we showed that the swarm centroid will approach the leader, now we have to find a bound on the ultimate swarm size to prove swarm stability. Let $e_i = x_i - \overline{x}$ denote the vector pointing from agent i to the swarm centroid. The following theorem asserts, that agent trajectories are globally uniformly ultimately bounded for an immobile leader. The global uniform ultimate boundedness of the agent trajectories is captured by the following theorem.

Theorem 2.4. *Consider a swarm consisting of N agents with dynamics (2.9), a leader agent with dynamics (2.10) and control input (2.4), where Assumptions 1 and 2 are satisfied. As $t \to \infty$, all swarm members will converge to a hyperball*

$$H^{\epsilon}(\overline{x}) = \{x_i : \|x_i - \overline{x}\| \leq \epsilon\},$$

where

$$\epsilon = \frac{(N-1)(\overline{F}^r + \frac{2}{N}\overline{F}_L^r)}{N\underline{k}^a + \underline{k}_L^a}.$$

Moreover, the convergence to any system state, where

$$\|e_i\| \leq \frac{(N-1)(\overline{F}^r + \frac{2}{N}\overline{F}_L^r)}{(N\underline{k}^a + \underline{k}_L^a)(1-\gamma)} := K_\gamma$$

for all $i = 1, 2, \cdots, N$ and $\gamma \in (0,1)$ occurs in finite time bounded by

$$T_\gamma = \max_{1 \leq i \leq N} \left\{ -\frac{1}{2\gamma(N\underline{k}^a + \underline{k}_L^a)} \ln\left(\frac{K_\gamma^2}{\|e_i(0)\|^2}\right) \right\}.$$

Proof. Consider the following Lyapunov-function candidate corresponding to agent i:

$$W_i(x) = \frac{1}{2} e_i^T e_i.$$

Taking the time derivative along the agent trajectory, in view of (2.9) yields

$$\dot{W}_i = u_i^T e_i - \dot{\overline{x}}^T e_i.$$

Taking Lemma 2.2 into account we have

$$\dot{W}_i = \Theta_1 + \Theta_2 + \Theta_3,$$

where

$$\Theta_1 = -\sum_{j=1}^{N} f_{i,j}(\|x_i - x_j\|)(x_i - x_j)^T e_i,$$

$$\Theta_2 = -f_{i,\mathrm{L}}(\|x_i - x_\mathrm{L}\|)(x_i - x_\mathrm{L})^T e_i,$$
$$\Theta_3 = \frac{1}{N}\sum_{j=1}^{N} f_{j,\mathrm{L}}(\|x_j - x_\mathrm{L}\|)(x_j - x_\mathrm{L})^T e_i.$$

Now we will find upper bounds for Θ_1, Θ_2 and Θ_3, and determine the region where the Lyapunov-function must decrease. This at the same time implies that agent i is getting closer to the centroid.

A bound for Θ_1 can be found by noticing that

$$\sum_{j=1}^{N}(x_i - x_j) = Nx_i - N\overline{x} = Ne_i.$$

Then, given Assumption 2 and the bounds on the attractive and repulsive forces, we can write

$$\Theta_1 \leq -Nk^\mathrm{a}\|e_i\|^2 + (N-1)\overline{F}^\mathrm{r}\|e_i\|. \tag{2.15}$$

For Θ_2, note that by using the notation from the proof of Lemma 2.3 we can expand $(x_i - x_\mathrm{L})$ as

$$(x_i - x_\mathrm{L}) = (x_i - \overline{x}) + (\overline{x} - x_\mathrm{L}) = e_i + \tilde{e}.$$

In view of this, and by substituting the attraction and repulsion components, Θ_2 takes the form

$$\Theta_2 = -k^\mathrm{a}_\mathrm{L}\|e_i\|^2 - k^\mathrm{a}_\mathrm{L}\tilde{e}^T e_i + f^\mathrm{r}_{i,\mathrm{L}}(\|x_i - x_\mathrm{L}\|)(x_i - x_\mathrm{L})^T e_i. \tag{2.16}$$

Lastly, since

$$\sum_{j=1}^{N}(x_j - x_\mathrm{L}) = N\tilde{e},$$

for Θ_3 we have

$$\Theta_3 = k^\mathrm{a}_\mathrm{L}\tilde{e}^T e_i - \frac{1}{N}\sum_{j=1}^{N} f^\mathrm{r}_{j,\mathrm{L}}(\|x_j - x_\mathrm{L}\|)(x_j - x_\mathrm{L})^T e_i. \tag{2.17}$$

As one may notice, the terms containing $\tilde{e}$ in (2.16) and (2.17) will cancel each other out. Moreover, the sum of the repulsion components in Θ_2 and Θ_3 can be written as

$$\frac{N-1}{N} f^\mathrm{r}_{i,\mathrm{L}}(\|x_i - x_\mathrm{L}\|)(x_i - x_\mathrm{L})^T e_i - \frac{1}{N}\sum_{j=1, j\neq i}^{N} f^\mathrm{r}_{i,\mathrm{L}}(\|x_j - x_\mathrm{L}\|)(x_j - x_\mathrm{L})^T e_i$$

$$\leq \frac{2}{N}(N-1)\overline{F}^{\mathrm{r}}_{\mathrm{L}}\|e_i\|.$$

Combining the bounds for Θ_1, Θ_2 and Θ_3 we then obtain

$$\dot{W}_i \leq \|e_i\| \left[(-Nk^{\mathrm{a}} - k^{\mathrm{a}}_{\mathrm{L}})\|e_i\| + (N-1)(\overline{F}^{\mathrm{r}} + \frac{2}{N}\overline{F}^{\mathrm{r}}_{\mathrm{L}}) \right]. \tag{2.18}$$

Since $\|e_i\| \geq 0$, the time derivative of the Lyapunov function (2.18) is negative, if

$$\|e_i\| > \frac{(N-1)(\overline{F}^{\mathrm{r}} + \frac{2}{N}\overline{F}^{\mathrm{r}}_{\mathrm{L}})}{N\underline{k}^{\mathrm{a}} + \underline{k}^{\mathrm{a}}_{\mathrm{L}}} \equiv \epsilon.$$

Decreasing W_i implies that the distance between agent i and the swarm centroid is decreasing as well, which is true for every agent $i = 1, 2, \cdots, N$. Therefore as $t \to \infty$, every member of the swarm must be within a hyperball around the centroid with radius ϵ.

Moreover, equation (2.18) with $A = N\underline{k}^{\mathrm{a}} + \underline{k}^{\mathrm{a}}_{\mathrm{L}}$ and $B = (N-1)(\overline{F}^{\mathrm{r}} + \frac{2}{N}\overline{F}^{\mathrm{r}}_{\mathrm{L}})$ yields that

$$\dot{W}_i \leq \|e_i\|(-A\|e_i\| + B).$$

Using the same arguments as in the proof of Lemma 2.3, if we assume that $\|e_i\| \geq \frac{B}{A(1-\gamma)} = K_\gamma$ we obtain

$$W_i(t) \leq W_i(0)\, \mathrm{e}^{-2\gamma A t}.$$

Solving the inequality for $\|e_i\| = K_\gamma$ and $W_i = \frac{1}{2}K_\gamma^2$ yields the time bound for agent i as

$$T^i_\gamma = \frac{1}{-2\gamma A} \ln \left[\frac{K^2_\gamma}{2W_i(0)} \right].$$

If we find T^i_γ with the slowest convergence, we obtain the result stated in Theorem 2.4. □

Remark 2.5. Theorem 2.4 provides an ultimate bound on the swarm size of the follower agents around the swarm centroid. Combining the results of Lemma 2.3 and Theorem 2.4, we can conclude that the ultimate bound on the swarm size of the follower agents and the leader is given by a hyperball with radius

$$E = \epsilon + \frac{\overline{F}^{\mathrm{r}}_{\mathrm{L}}}{\underline{k}^{\mathrm{a}}_{\mathrm{L}}}.$$

Remark 2.6. The presented time bound is determined by the agent for which $\|e_i(0)\|$ is the largest. That is, the slowest convergence among all agents occurs for the one initially furthest away from the swarm centroid, which matches our expectations.

Theorem 2.4 reflects the possibility of putting adjustable autonomy into practice by manipulating the swarms size through some time-varying parameters. Intuitively, the swarm size is proportional to the repulsion and decreases with high attractive force. We also mention, that the introduced theorem provides a conservative bound on the swarm size, which originates in the nature of the proof presented. As one may see in Section 2.5, the ultimate swarm size in fact is smaller than Theorem 2.4 suggests.

In this section we considered an immobile leader to demonstrate our results. However, by applying a simple coordinate transformation, all the introduced results hold for a leader in motion as well. In fact, letting

$$x_i' = x_i - x_{\mathrm{L}}$$

and

$$\dot{x}_i' = u_i' = -\nabla_{x_i} V(x) - \dot{x}_{\mathrm{L}}$$

for all $i = 1, 2, \cdots, N$, allows for the results in this section to be applied to systems with non-static leaders.

So far we have investigated the boundedness of the leader-centroid distance and the agent-centroid distance affected by time-varying attraction and repulsion. In Theorem 2.4 a hyperball is defined bounding $\|e_i\|$, the individual agents' distance from the centroid. A slightly different approach is to analyze the sum of squared distances from the centroid to every agent in the swarm, which serves as a combined bound. The next proposition reflects this collective formulation of the problem.

Proposition 2.7. *Consider a swarm consisting of N agents with dynamics (2.9), a leader agent with dynamics (2.10) and control input (2.4), where Assumptions 1 and 2 are satisfied. As $t \to \infty$, the sum of squared distances from the centroid will converge to a hyperball*

$$H^*(\overline{x}) = \{x : \sum_{1 \le i \le N} \|x_i - \overline{x}\|^2 \le \epsilon_*^2\},$$

where

$$\epsilon_* = \sqrt{N} \cdot \frac{(N-1)\overline{F}^r + \overline{F}_L^r}{N\underline{k}^a + \underline{k}_L^a}.$$

Proof. Let the Lyapunov-function corresponding to agent i be $W_i(x) = \frac{1}{2} e_i^T e_i$ and $W = \sum_{i=1}^N W_i(x)$. From the proof of Theorem 2.4, we have the inequality

$$\dot{W}_i \le -Nk^{\mathrm{a}}\|e_i\|^2 + (N-1)\overline{F}^{\mathrm{r}}\|e_i\| - k_{\mathrm{L}}^{\mathrm{a}}\|e_i\|^2 - k_{\mathrm{L}}^{\mathrm{a}}\tilde{e}^T e_i + f_{i,\mathrm{L}}^{\mathrm{r}}(\|x_i - x_{\mathrm{L}}\|)(x_i - x_{\mathrm{L}})^T e_i$$

$$+\frac{1}{N}\sum_{j=1}^{N} f_{j,\mathrm{L}}(\|x_j - x_\mathrm{L}\|)(x_j - x_\mathrm{L})^T e_i.$$

One may notice, that

$$\sum_{i=1}^{N} k_\mathrm{L}^\mathrm{a}\tilde{e}^T e_i = k_\mathrm{L}^\mathrm{a}\tilde{e}^T \sum_{i=1}^{N} e_i = 0$$

and along similar lines

$$\sum_{i=1}^{N}\frac{1}{N}\sum_{j=1}^{N} f_{j,\mathrm{L}}(\|x_j - x_\mathrm{L}\|)(x_j - x_\mathrm{L})^T e_i = \frac{1}{N}\sum_{i=1}^{N} e_i^T \sum_{j=1}^{N} f_{j,\mathrm{L}}(\|x_j - x_\mathrm{L}\|)(x_j - x_\mathrm{L}) = 0.$$

Therefore, we have

$$\dot{W} \leq -Nk^\mathrm{a}\sum_{i=1}^{N}\|e_i\|^2 + (N-1)\overline{F}^\mathrm{r}\sum_{i=1}^{N}\|e_i\| - k_\mathrm{L}^\mathrm{a}\sum_{i=1}^{N}\|e_i\|^2 + \overline{F}_\mathrm{L}^\mathrm{r}\sum_{i=1}^{N}\|e_i\|.$$

Applying the notation $\sqrt{\sum_{i=1}^{N}\|e_i\|^2} = \|e\|$, observe that $\sum_{i=1}^{N}\|e_i\| \leq \|e\|\cdot\sqrt{N}$, which yields

$$\dot{W} \leq \|e\|\cdot\left[(-Nk^\mathrm{a} - k_\mathrm{L}^\mathrm{a})\|e\| + \overline{F}^\mathrm{r}(N-1)\sqrt{N} + \overline{F}_\mathrm{L}^\mathrm{r}\sqrt{N}\right]. \tag{2.19}$$

Due to the fact that $W = \frac{1}{2}\|e\|^2$ and using the same reasoning as in the proof of Theorem 2.4 for (2.18) applied to (2.19) we arrive at the bound ϵ_* in the proposition. □

2.4 Robust aggregation with general dynamics

Next, we build on the results from the previous section and modify the introduced framework to accommodate for agents with uncertain higher order dynamics. The ideas and derivation presented here extend well known results from the literature [44] to time-varying virtual interaction forces.

Consider the same framework introduced in Section 2.2, but now with the following agent dynamics:

$$M_i(x_i)\ddot{x}_i + g_i(x_i, \dot{x}_i) = u_i, \tag{2.20}$$

where $M_i \in \mathbb{R}^{nxn}$ is the inertia matrix of agent i and g_i represents some additional effects such as damping, disturbances or gravitational effects. We allow for the inertia of each agent to be an unknown parameter, but the following assumptions must hold.

Assumption 3. For all agents $i = 1, 2, \cdots, N$ we have

$$\underline{M_i}\|y^2\| \leq y^T M_i(x_i) y \leq \overline{M_i}\|y^2\| < \infty$$

for real scalars

$$0 < \underline{M_i} < \overline{M_i} < \infty,$$

and any arbitrary column vector $y \in \mathbb{R}^n$.

In order to reflect model uncertainties in the agent dynamics, we will assume that g_i consists of a known part g_i^{k} and a bounded unknown part g_i^{u}.

Assumption 4. For all $g_i(x_i, \dot{x_i})$ $i = 1, 2, \cdots, N$ the equality

$$g_i(x_i, \dot{x_i}) = g_i^{\mathrm{k}}(x_i, \dot{x_i}) + g_i^{\mathrm{u}}(x_i, \dot{x_i})$$

is satisfied. Furthermore, a state-dependent upper bound exists such that

$$\|g_i^{\mathrm{u}}(x_i, \dot{x_i})\| \leq G_i(x_i, \dot{x_i}).$$

Due to the second-order dynamics analyzed in this section, we have to add assumptions regarding the time-derivative of attraction and repulsion components.

Assumption 5. For all $t \geq 0$ the following inequalities must stand,

$$\begin{aligned}
\dot{k}^{\mathrm{a}}(t) &\leq \Gamma_a(x), \\
\dot{k}_{\mathrm{L}}^{\mathrm{a}}(t) &\leq \Gamma_a^{\mathrm{L}}(x), \\
\dot{f}_{i,j}^{\mathrm{r}}(\|x_i - x_j\|, t)\|x_i - x_j\| &\leq \Gamma_r(x) \quad \text{for all } i, j, \\
\dot{f}_{i,\mathrm{L}}^{\mathrm{r}}(\|x_i - x_{\mathrm{L}}\|, t)\|x_i - x_{\mathrm{L}}\| &\leq \Gamma_r^{\mathrm{L}}(x) \quad \text{for all } i,
\end{aligned}$$

where $\Gamma_a, \Gamma_a^{\mathrm{L}}, \Gamma_r, \Gamma_r^{\mathrm{L}}$ are known, state-dependent, finite upper bounds.

Although we assume state-dependent bounds, it is sufficient to provide global bounds for the attraction and repulsion term derivatives.

The next assumption we make is a smoothness assumption on the artificial potentials, which is satisfied by a wide class of functions in practice. Moreover, we know these bounds during the design of the control law, since the artificial potential functions are determined by the system designer.

Assumption 6. For all $\{i,j\}$ pairs, where $i = 1,2,\cdots,N$ and $j = 1,2,\cdots,N$ the potential function gradients are bounded as follows:

$$\|\nabla_{x_i} V(x)\| \leq \alpha(x) \quad \text{for all } x_i$$
$$\|\nabla_{x_j} [\nabla_{x_i} V(x)]\| \leq \beta(x) \quad \text{for all } x_i \text{ and } x_j,$$

where $\alpha(x)$ and $\beta(x)$ are known and finite functions of the agent states.

The last assumption we need states that the agents are initially motionless.

Assumption 7. $\dot{x}_i(0) = 0$ for $i = 1,2,\cdots,N$.

In Section 2.3 we showed that if agent movement is governed by (2.9), then we have an ultimate bound on the swarm size and some other properties hold. Sliding mode control reduces the motion of the system to a lower dimensional sliding manifold, hence in our case forcing it to move according to single-integrator agent dynamics [45, 46]. By showing that the sliding mode occurs in finite time, we also prove that all the results and conclusion from Section 2.3 hold for the more general dynamics introduced in this section.

Theorem 2.8. *Consider a swarm consisting of N members with dynamics (2.20), an artificial potential function satisfying Assumptions 1, 2, 5, 6, and initial conditions as prescribed in Assumption 7. Let the control input for agent i be*

$$u_i = -K_i(x)\,\mathrm{sign}(s_i) + g_i^k(x_i, \dot{x}_i), \tag{2.21}$$

with gain

$$K_i(x) > \overline{M}_i\left(\frac{1}{\underline{M}_i} G_i(x_i, \dot{x}_i) + \overline{J}_i(x) + \varepsilon_i\right) \tag{2.22}$$

for some $\varepsilon_i > 0$, where

$$\overline{J}_i(x) = N\beta(x)\,[\alpha(x(0)) + \alpha(x)] + \|x_i - x_L\|\Gamma_a^L(x) + \Gamma_r^L(x) + (N-1)\left[\max_{1\leq j\leq N} \|x_i - x_j\|\Gamma_a(x) + \Gamma_r(x)\right], \tag{2.23}$$

and sliding manifold

$$s_i = \dot{x}_i + \nabla_{x_i} V(x). \tag{2.24}$$

Then, the sliding mode occurs in all s_i surfaces and

$$\dot{x}_i = -\nabla_{x_i} V(x)$$

is satisfied in finite time, bounded by

$$T_s = \max_{1\leq i\leq N}\left\{\frac{\|\nabla_{x_i}V(x(0))\|}{\varepsilon_i}\right\}. \tag{2.25}$$

Proof. The reaching condition of sliding mode control states that the sliding mode occurs in finite time, if

$$s_i^T\dot{s}_i < -\varepsilon_i\|s_i\| \tag{2.26}$$

for some $\varepsilon_i > 0$. Considering the Lyapunov function candidate $L_i = \frac{1}{2}s_i^T s_i$ we have $\dot{L}_i < -\varepsilon_i\|s_i\|$. From here, by applying the *comparison principle* [45] one can show that the inequality is satisfied in finite time bounded by $T_s^i = \frac{\|s_i(0)\|}{\varepsilon_i}$, where $\|s_i(0)\| = \|\nabla_{x_i}V(x(0))\|$ due to Assumption 7. The time bound is determined by the maximum of all T_s^i individual time bounds, which proves (2.25).

From (2.20) and in view of our definition of the sliding manifold in (2.24) we obtain

$$s_i^T\dot{s}_i = s_i^T\left[M_i(x_i)^{-1}u_i - M_i(x_i)^{-1}g_i(x_i,\dot{x}_i) + \frac{d}{dt}\nabla_{x_i}V(x)\right]. \tag{2.27}$$

First we derive an upper bound for the right-hand side, then show that (2.26) can always be satisfied. Applying the chain rule, we have

$$\begin{aligned}\frac{d}{dt}\nabla_{x_i}V(x) = &\sum_{j=1}^{N}\nabla_{x_j}\left[\nabla_{x_i}V(x)\right]\dot{x}_j + \sum_{j=1}^{N}\dot{k}^{\mathrm{a}}(x_i - x_j)\\ &- \sum_{j=1}^{N}\dot{f}^{\mathrm{r}}_{i,j}(\|x_i - x_j\|,t)(x_i - x_j) + \dot{k}^{\mathrm{a}}_{\mathrm{L}}(x_i - x_{\mathrm{L}}) - \dot{f}^{\mathrm{r}}_{i,\mathrm{L}}(\|x_i - x_{\mathrm{L}}\|,t)(x_i - x_{\mathrm{L}}).\end{aligned} \tag{2.28}$$

In view of Assumption 6 and 7 it is shown in [43] that

$$\|\sum_{j=1}^{N}\nabla_{x_j}\left[\nabla_{x_i}V(x)\right]\dot{x}_j\| \leq N\beta(x)\left(\alpha(x(0)) + \alpha(x)\right).$$

If we take Assumption 5 into account and apply the *Cauchy-Schwarz inequality* we have the state-dependent upper bound from (2.23):

$$\|\frac{d}{dt}\nabla_{x_i}V(x)\| \leq \overline{J}_i(x).$$

Now choose the control input for agent i as in (2.21), where *sign* operates elementwise on s_i. Notice, that

$$s_i^T \operatorname{sign}(s_i) = |s_{i_1}| + |s_{i_2}| + \cdots + |s_{i_n}| \geq \|s_i\|.$$

Therefore by substituting (2.21) into (2.27) and applying the bounds from Assumptions 3, 4 and the bound we derived for $\|\frac{d}{dt}\nabla_{x_i} V(x)\|$ yields

$$s_i^T s_i \leq -\|s_i\| \left(\frac{1}{\overline{M}_i} K_i(x) - \frac{1}{\underline{M}_i} G_i(x_i, \dot{x_i}) - \overline{J}_i(x) \right). \tag{2.29}$$

If we let the inequality from (2.22) hold, then the reaching condition (2.26) is satisfied, thus the sliding mode occurs in finite time. □

2.5 Simulation

The proposed results are verified in this section using numerical simulations. Consider the case with $N = 15$, and an immobile leader fixed at the origin. The initial agent locations were chosen randomly within a radius of $R = 30$ around the point $P = (40, 40)$. The agent states evolve in $\mathbb{R}^2$ governed by the underlying potential function in (2.7) and the corresponding forces of attraction and repulsion in (2.8). It is straightforward to prove that in this case

$$\overline{F}^{\mathrm{r}} = \overline{k}^{\mathrm{r}} \sqrt{\frac{r}{2e}}$$

and

$$\overline{F}_{\mathrm{L}}^{\mathrm{r}} = \overline{k}_{\mathrm{L}}^{\mathrm{r}} \sqrt{\frac{r_{\mathrm{L}}}{2e}}.$$

The simulations were performed under two different agent dynamics.

2.5.1 Single-integrator (SI) dynamics

Consider the agent dynamics in (2.9), with $n = 2$ and the following attraction-repulsion parameters: $k^{\mathrm{a}} = 2, k_r = 3, r = 2, k_{\mathrm{L}}^{\mathrm{a}} = 10.1 + 10\sin(\frac{2\pi}{T} f t), f = 4, k_{\mathrm{L}}^{\mathrm{r}} = 20.2, r_{\mathrm{L}} = 0.1$ where $T = 200$ is the simulation time length. We assume the states of the agents provide their coordinates in the cartesian x-y plane.

The agent trajectories under the control (2.4) are illustrated in Fig. 2.1(a). As one may observe, the agents approach the origin and aggregate in the proximity of each other and the leader. The ultimate swarm size ϵ is marked by a dashed circle centered at the swarm centroid at $t = T$ in

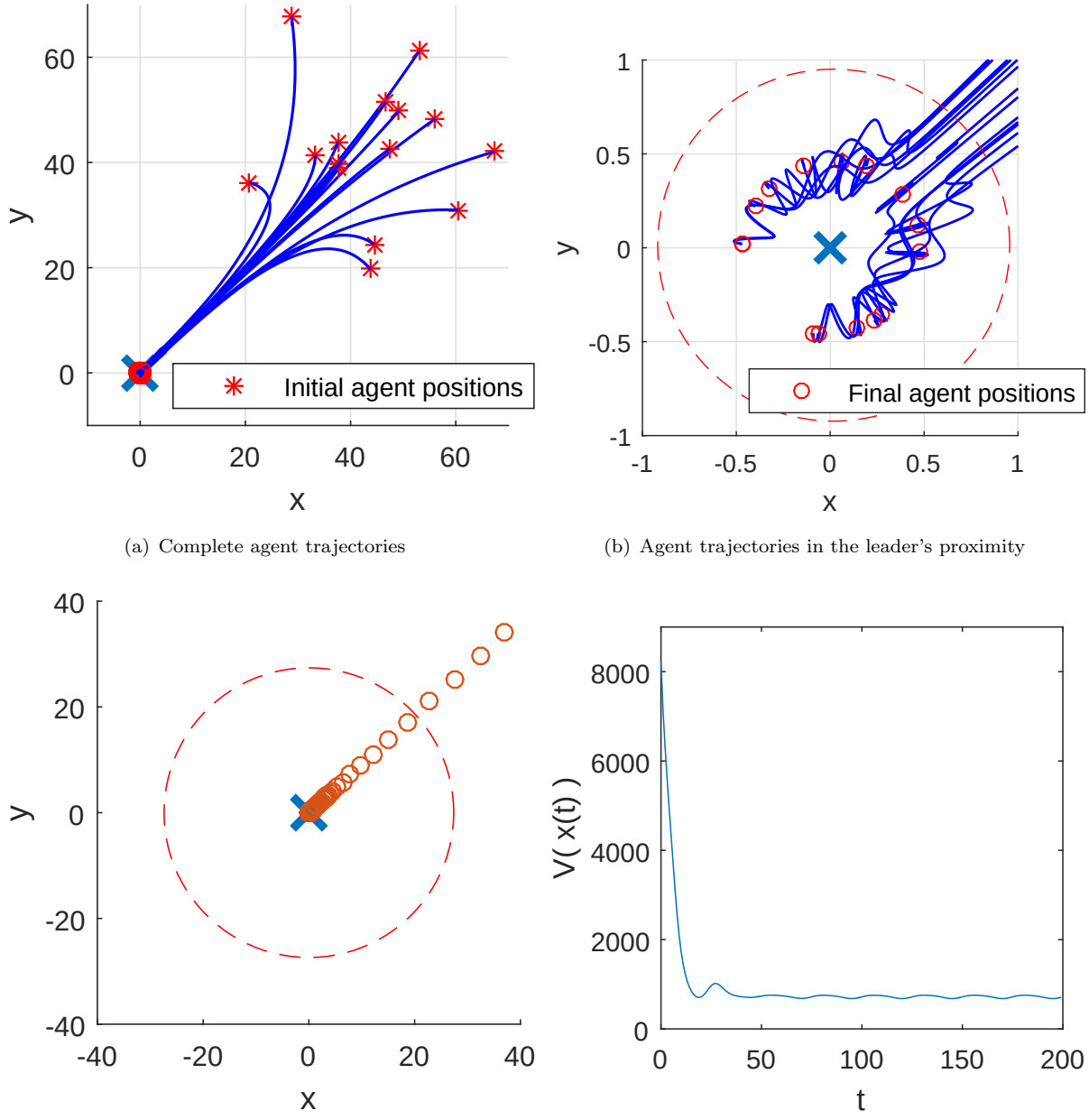

(a) Complete agent trajectories

(b) Agent trajectories in the leader's proximity

(c) Centroid locations in equal time intervals

(d) Global objective function

Figure 2.1: Agent motion with SI dynamics

Fig. 2.1(b). The agents enter the region as specified in Theorem 2.4 and never leave it, even though the leader attractive force is time-varying. As mentioned in Section 2.3, Theorem 2.4 provides a conservative bound on the region of attraction. The actual time-varying swarm size fits in a smaller region.

As the leader attraction varies in time, the swarm size changes dynamically, while preserving its cohesion. As shown in Fig. 2.1(c), the swarm centroid approaches the leader and the convergence

speed is inversely proportional to the centroid-leader distance. The dashed circle marks the upper bound for $\|\tilde{e}\|$ analyzed in Lemma 2.3. In this particular case, the leader attractive force is stronger than the inter-agent cohesion forces, therefore the swarm centroid is drawn to the leader's location. Taking a look at the value of the potential function from (2.7) in Fig. 2.1(d), the speed of the algorithm can be observed. The global objective function does not converge to a single value due to the variations in interaction forces, but oscillates within a bounded interval.

2.5.2 Double-integrator (DI) dynamics

Consider $N = 10$ agents with double integrator dynamics, that is

$$M_i \ddot{x}_i = u_i,$$

where M_i denotes the mass of agent i. In the simulation plotted in Figs. 2.2(a) and 2.2(b) the value of $M_i = 1$ was used for the sake of simplicity. All other system parameters remained unchanged from the single integrator case in the previous subsection. The control gain $K_i(x)$ was derived from the bounds

$$\begin{aligned}\alpha(x) &= N\left[\overline{k}^{\mathrm{a}} \max_{1\le j\le N}\|x_i - x_j\| + k^{\mathrm{r}}\sqrt{\frac{r}{2}}\mathrm{e}^{-\frac{1}{2}}\right] \quad + \|x_i - x_L\|\overline{k}^{\mathrm{a}}_{\mathrm{L}} + k^{\mathrm{r}}_{\mathrm{L}}\sqrt{\frac{r_{\mathrm{L}}}{2}}\mathrm{e}^{-\frac{1}{2}}\,,\\ \beta(x) &= N\left[\overline{k}^{\mathrm{a}} + 2k^{r}\mathrm{e}^{-\frac{1}{2}}\right] + \overline{k}^{\mathrm{a}}_{\mathrm{L}} + 2k^{r}_{\mathrm{L}}\mathrm{e}^{-\frac{1}{2}}\,,\end{aligned}$$

presented in [43] (extended with the leader interaction term) and from the *a priori* known bound on the time-derivative of the leader attraction term.

As one may observe, the agents approach the leader and remain within the region determined by Theorem 2.4 (dashed circle), thus the results for the single integrator model still hold.

2.5.3 Double-integrator dynamics with model uncertainty

This section presents simulation results for a more realistic case, where the agent dynamics contain an unknown but bounded part representing disturbances and model uncertainties. In particular let

$$M_i \ddot{x}_i + g^{\mathrm{u}}(\dot{x}_i) = u_i,$$

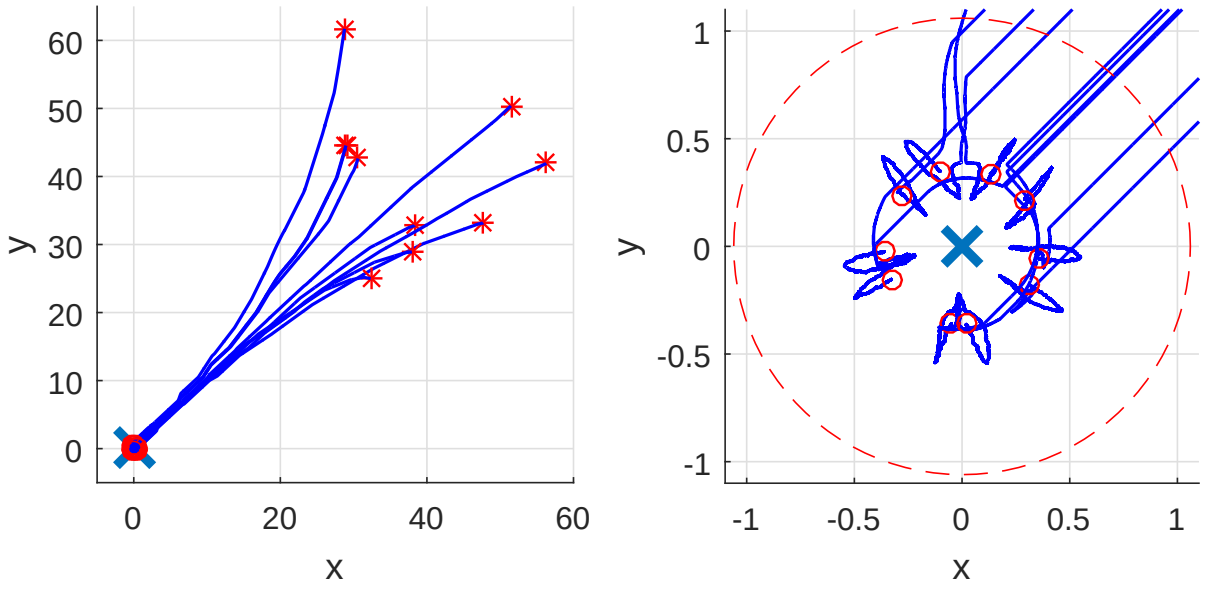

(a) Complete agent trajectories

(b) Agent trajectories in the leader's proximity

Figure 2.2: Agent motion with DI dynamics

where $g^{\mathrm{u}}(\dot{x}_i)$ represents the unknown part such that

$$g^{\mathrm{u}}(\dot{x}_i) = \begin{cases} h^{\mathrm{u}}\dot{x}_i & \|g^{\mathrm{u}}(\dot{x}_i)\| \leq G_{\max} \\ h^{\mathrm{u}}\dot{x}_i \cdot \frac{G_{\max}}{\|h^{\mathrm{u}}\dot{x}_i\|} & \|g^{\mathrm{u}}(\dot{x}_i)\| > G_{\max}. \end{cases}$$

For the included numerical example $M_i = 1$, $h^{\mathrm{u}} = 0.5$ and $G_{\max} = 10$ values were used. The simulation was performed for $N = 10$ agents initially scattered within a circle of radius $R = 20$ centered at the point $P = (10, 10)$. The attraction repulsion parameters were identical to the DI case. Apart from $G_{\max}$ included in the control input (see (2.21) and (2.22)), no other information about $g^{\mathrm{u}}(\dot{x}_i)$ was used to control the multi-agent system.

The simulation results show, that the proposed control technique was able to drive the agents to the proximity of the leader (see Figs. 2.3(a) and 2.3(b)). However, compared to the ideal DI case, one may observe an overshoot in the agent trajectories. The deviation from an "optimal" route, as seen in the DI simulations, is the result of the unknown first-order term in the agent dynamics.

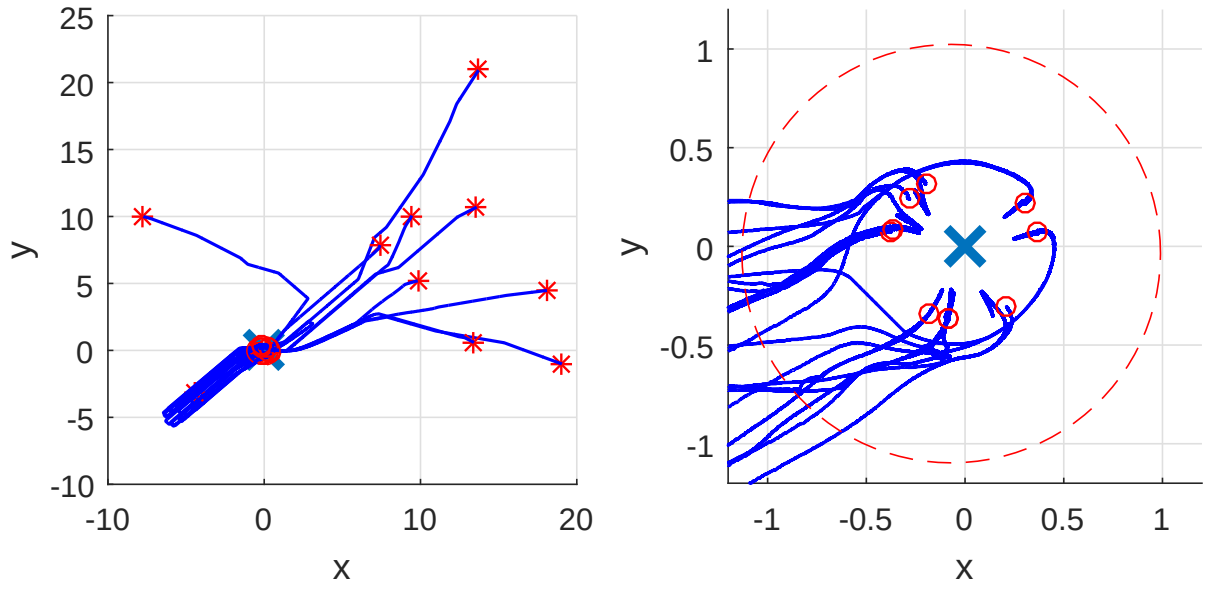

(a) Complete agent trajectories with model uncertainty

(b) Agent motion in the leader's proximity

Figure 2.3: Agent motion with DI dynamics and model uncertainty

2.6 Conclusions

In this chapter, the aggregation and leader tracking problem was studied for multi-agent systems with time-varying artificial potential functions. The time-dependent parameters of the artificial potential function was introduced as a potential framework for incorporating varying autonomy level of follower agents in the control of swarms. For single integrator agents, it was demonstrated that the swarm aggregate around the leader and the agents' trajectories are bounded. These results were then extended to agents with higher order dynamics. Numerical examples were also provided here to illustrate the results of our theoretical derivation.

Chapter 3

Coordinated control under balanced communication graph

3.1 Introduction

The idea of adjusting the interaction rules between the leader and the follower agents of a swarm was introduced in the previous chapter and in [42]. The intent was to provide the follower agents greater autonomy if leader performance declined. The proposed framework involves time-varying social potential functions acting between the agents and the leader in a complete graph structure. That is, each follower imposes both attraction and repulsion to every other agent and is affected by the leader's interaction forces. Gazi and Passino extensively investigated swarm models with global coupling and unit coupling weights [13, 16, 44, 47]. Relaxing the assumption on the communication graph would constitute a significant step towards practical implementation of our proposed framework on a robotic system.

The influence of information topology on multi-agent system stability is an important research focus in the area of swarm coordination. In most works, algebraic graph theory is deployed to address this problem. Olfati-Saber and Murray [48] analyzed the consensus problem with strongly connected switching topology and considered the effect of time delay. Sepulchre *et al.* [49] investigated the planar motion of particles exchanging relative information, focusing on balanced communication. Li[38] discussed the stability and boundary of single integrator swarms with general, directed topology generalizing the results of Gazi and Passino.

Algebraic connectivity is a spectral property of graphs, quantifying connectedness. A remarkable finding of the field is the influence of the algebraic connectivity of the communication graph on

the speed of convergence in consensus problems [48]. Due to its impact on the properties of dynamic systems operating over an information network, the effect of graph parameters on the algebraic connectivity was studied extensively. Kim and Mesbahi [50] aimed at maximizing the algebraic connectivity of weighted graphs by finding the optimal vertex positional configuration. Bounds on the algebraic connectivity as a function of graph parameters can be found in [51] and [52].

In this chapter we aim at extending the control framework for leader-follower swarms with time varying inter-agent dynamics from the previous chapter and [42], to balanced directed communication topologies. The proposed control framework allows uncorrelated time-varying inter-agent attraction and repulsion coupling weights, which are not uniform among all follower agents. Swarm centroid motion and leader-centroid ultimate distance is analyzed under these conditions, and we establish a relationship between the bounds on the time-varying coupling weights and the ultimate swarm size. Next, the swarm control problem with time-varying inter-agent dynamics is extended to systems with switching communication topologies. Using the properties of algebraic connectivity of weighted graphs, an analytic expression of the ultimate swarm formation size is determined in the presence of the time-varying system parameters and configuration. Applications of this switching topology control framework are briefly discussed, such as swarm cohesion maintenance or collision avoidance.

The organization of the chapter is as follows. Section 1.2 introduces the necessary concepts in graph theory. Framework description and stability analysis is performed in Section 3.2, including centroid motion, leader-centroid distance and ultimate swarm size. Section 3.3 is a discussion on the possible applications of the introduced framework. Numerical simulations are presented in Section 3.4 to demonstrate our results. We draw conclusions in Section 3.5.

3.2 Stability analysis under balanced, time-varying coupling weights

3.2.1 Framework description

We adopt the framework introduced in [42] with a relaxed communication topology and coupling matrix as discussed in [38]. Consider a swarm involving N agents and a leader. We will denote the states of agent i with the column vector $x_i \in \mathbb{R}^n$ and the states of the leader agent with the column vector $x_L \in \mathbb{R}^n$. Let u_i denote the control input to agent i. The system evolves in the n-dimensional Euclidean space governed by the motion equations

$$\dot{x_i} = u_i, \tag{3.1}$$

with control input

$$u_i = \sum_{j=1,j\neq i}^{N} \left[-f_{ij}^a(x_i,x_j,t) + f_{ij}^r(x_i,x_j,t)\right] - f_{L,i}^a(x_i,x_L,t) + f_{L,i}^r(x_i,x_L,t), \tag{3.2}$$

where f_{ij}^a and f_{ij}^r denote the attraction and repulsion functions from agent j to i; $f_{L,i}^a$ and $f_{L,i}^r$ describes the attraction and repulsion from the leader to agent i. Furthermore, we will assume linear long-range attraction and nonlinear short-range upper-bounded repulsion, with time-varying coupling strengths as

$$\begin{aligned} f_{ij}^a &= w_{ij}(t)(x_i - x_j), \\ f_{ij}^r &= \nu_{ij}(t) g^r(\|x_i - x_j\|)(x_i - x_j), \\ f_{L,i}^a &= w_{L,i}(t)(x_i - x_L), \\ f_{L,i}^r &= \nu_{L,i}(t) g_L^r(\|x_i - x_L\|)(x_i - x_L), \end{aligned} \tag{3.3}$$

where $w_{ij}(t) \geq 0, \nu_{ij}(t) \geq 0$ are the attraction and repulsion coupling weights from agent j to i; $w_{L,i}(t) \geq 0, \nu_{L,i}(t) \geq 0$ denote the leader-agent attraction and repulsion coupling weights; $g^r(\|x_i - x_j\|) : \mathbb{R}^n \mapsto \mathbb{R}, \quad g_L^r(\|x_i - x_L\|)\mathbb{R}^n \mapsto \mathbb{R}$ are the repulsion terms such that the following assumption holds.

Assumption 8. There exist constants $F^r > 0$ and $F_L^r > 0$ such that

$$0 < g^r(\|y\|)\|y\| \leq F^r \quad \forall t > 0$$

$$0 < g_L^r(\|y\|)\|y\| \leq F_L^r \quad \forall t > 0.$$

Let $W(t) = [w_{ij}(t)] \in \mathbb{R}^{N\times N}$ be the time dependent attraction coupling matrix of the swarm, where $w_{ij}(t) \geq 0$ for $t \geq 0$ and $i \neq j$, and $w_{ii}(t) = -\sum_{j=1,j\neq i}^{N} w_{ij}(t) < 0$. Notice, that the diagonal elements of W do not affect the swarm dynamics. Here, $w_{ij} = 0$ means that agents i and j are not connected, whereas $w_{ij} > 0$ indicates attraction from agent j to i with coupling force w_{ij}. Analogously, let $K(t) = [\nu_{ij}(t)] \in \mathbb{R}^{N\times N}$ be the repulsion coupling matrix of the swarm, where $\nu_{ij}(t) \geq 0$ for $t \geq 0$ and $i \neq j$, and $\nu_{ii}(t) = -\sum_{j=1,j\neq i}^{N} \nu_{ij}(t) < 0$. Denote $W_L(t) = [w_{L,1}(t)\ w_{L,2}(t)\ ...\ w_{L,N}(t)]^T \in \mathbb{R}^N$ the vector of leader attraction, and $K_L(t) = [\nu_{L,1}(t)\ \nu_{L,2}(t)\ ...\ \nu_{L,N}(t)]^T \in \mathbb{R}^N$ the vector of leader repulsion.

Let the weighted digraph G_a on $N+1$ vertices denote the *attraction graph* of the swarm, where a directed edge from j to i exists with edge-weight $w_{ij}(t)$ if $w_{ij}(t) > 0$. A directed edge from the leader to agent i exists if $w_{L,i} > 0$. Let the *repulsion graph* of the swarm represented by weighted digraph G_r on $N+1$ vertices, a directed edge from j to i exists with edge-weight $\nu_{ij}(t)$

if $\nu_{ij}(t) > 0$. Moreover, a directed edge from the leader to agent i exists is $\nu_{L,i} > 0$. One may notice that $L(G_a) = -W$ and $L(G_r) = -K$. Moreover, if the diagonal elements of W and K are omitted, we obtain the adjacency matrices of G_a and G_r.

First, we will investigate swarm properties under fixed communication topology, hence we introduce the following assumption.

Assumption 9. Denote E^a and E^r the edge sets of the attraction and repulsion graphs respectively. $E^a(0) = E^a(t) \quad \forall t > 0, E^r(0) = E^r(t) \quad \forall t > 0$.

We let the edge-weights to be time-varying, but bounded by known, positive bounds.

Assumption 10.

- For any agents i and j, there exist $\underline{w}_{ij} \geq 0$ and $\overline{w}_{ij} \geq 0$ such that $\underline{w}_{ij} \leq w_{ij}(t) \leq \overline{w}_{ij} \quad \forall t \geq 0$,
- For any agents i and j, there exist $\underline{w}_{L,i} \geq 0$ and $\overline{w}_{L,i} \geq 0$ such that $\underline{w}_{L,i} \leq w_{L,i}(t) \leq \overline{w}_{L,i} \quad \forall t \geq 0$,
- For any agents i and j, there exist $\underline{\nu}_{ij} \geq 0$ and $\overline{\nu}_{ij} \geq 0$ such that $\underline{\nu}_{ij} \leq \nu_{ij}(t) \leq \overline{\nu}_{ij} \quad \forall t \geq 0$,
- For any agents i and j, there exist $\underline{\nu}_{L,i} \geq 0$ and $\overline{\nu}_{L,i} \geq 0$ such that $\underline{\nu}_{L,i} \leq \nu_{L,i}(t) \leq \overline{\nu}_{L,i} \quad \forall t \geq 0$.

Denote

$$\begin{aligned}
\underline{W} &= [\underline{w}_{ij}] \in \mathbb{R}^{N\times N}, \\
\overline{K}_L &= [\overline{\nu}_{L,1}\ \overline{\nu}_{L,2}\ ...\ \overline{\nu}_{L,N}]^T \in \mathbb{R}^N, \\
\underline{\omega} &= \min_i \underline{w}_{L,i} \in \mathbb{R}, \\
\overline{\Lambda} &= \text{diag}(-\overline{\nu}_{11}, -\overline{\nu}_{22}, ..., -\overline{\nu}_{NN}) \in \mathbb{R}^{N\times N}, \\
\overline{\nu}_{ii} &= -\sum_{j=1, j\neq i}^{N} \overline{\nu}_{ij} \in \mathbb{R}.
\end{aligned}$$

Cohesion of an artificial swarm described in (3.1) with control input in (3.2) may only be maintained if the attraction graph is strongly connected and balanced.

Assumption 11. Let G^a be strongly connected and balanced for all $t > 0$,

$$\sum_{j=1, j\neq i}^{N} w_{ij} = \sum_{j=1, j\neq i}^{N} w_{ji}, \ i = 1, 2, ..., N+1.$$

Remark 3.1. W is irreducible as a result of Assumption 11. We also mention, that symmetric coupling is a special case of balanced coupling, where $w_{ij}(t) = w_{ji}(t), \quad \forall t > 0$.

For now, we will assume that the leader is immobile and fixed in the origin. However, all the introduced results hold for a leader in motion by applying the coordinate transformation $x_i' = x_i - x_L$. In our model the leader position indicates the point-of-interest to followers, therefore it is assumed that leader attraction acts on every agent.

Assumption 12. The leader is fixed in the origin, that is $x_L = 0$ and $\dot{x}_L = 0$.

Assumption 13. Leader attraction acts on every agent, that is

$$w_{L,i}(t) \geq 0, \quad i = 1, 2, ..., N \quad \forall t \geq 0.$$

Furthermore, let $w_{L,i}(t) = \omega_L(t), \quad i = 1, 2, ..., N \quad \forall t \geq 0$.

3.2.2 Motion of the swarm centroid

Define the swarm centroid as

$$\overline{x} = \frac{1}{N} \sum_{i=1}^{N} x_i. \tag{3.4}$$

In [16] Gazi *et al.* proves that the swarm centroid is stationary if no leader is present and both the attraction and repulsion graphs are complete, with unitary weights. However, in our framework the centroid movement is governed by nonlinear terms and the leader interaction.

Proposition 3.2. *Consider a swarm of N agents with dynamics (3.1) and a leader with dynamics as in Assumption 12 and coupling matrices $W(t)$ and $K(t)$, where Assumption 11 is satisfied. Then the motion of the swarm centroid is governed by*

$$\begin{aligned}\dot{\overline{x}} =& \frac{1}{N} \sum_{i=1}^{N} \sum_{j=1, j\neq i}^{N} \nu_{ij} g^r(\|x_i - x_j\|)(x_i - x_j) - \frac{1}{N} \sum_{i=1}^{N} w_{L,i}(x_i - x_L) \\ &+ \frac{1}{N} \sum_{i=1}^{N} \nu_{L,i}\ g_L^r(\|x_i - x_L\|)(x_i - x_L).\end{aligned}$$

Proof. From (3.1) and (3.4) we have

$$\dot{\overline{x}} = \frac{1}{N} \sum_{i=1}^{N} \dot{x}_i,$$

$$= -\frac{1}{N}\sum_{i=1}^{N}\sum_{j=1}^{N} w_{ij}(t)(x_i - x_j) + \frac{1}{N}\sum_{i=1}^{N}\sum_{j=1,j\neq i}^{N} \nu_{ij}(t) g^r(\|x_i - x_j\|)(x_i - x_j)$$
$$- \frac{1}{N}\sum_{i=1}^{N} w_{L,i}(t)(x_i - x_L) + \frac{1}{N}\sum_{i=1}^{N} \nu_{L,i}(t) g_L^r(\|x_i - x_L\|)(x_i - x_L).$$

Due to Assumption 11 and the definition of the diagonal elements in W we have $\sum_{i=1}^{N} w_{ij} = \sum_{i=1}^{N} w_{ji} = 0$, and therefore

$$\sum_{i=1}^{N}\sum_{j=1}^{N} w_{ij}(t)(x_i - x_j) = \sum_{i=1}^{N} x_i \sum_{j=1}^{N} w_{ij} - \sum_{j=1}^{N} x_j \sum_{j=1}^{N} w_{ij} = 0,$$

which completes the proof. □

Remark 3.3. The centroid motion is exclusively governed by the leader's attraction and repulsion in case of symmetric coupling.

3.2.3 Leader-centroid distance

In the context of leader-follower swarms, there are two characteristic properties to be analyzed. Swarm cohesion can be described by the swarm size, measured as an average deviation from the swarm centroid. On the other hand, the leader-swarm relationship is described by the *leader-centroid distance*, $\|\tilde{e}\|$, where $\tilde{e} = \overline{x} - x_L$.

Proposition 3.4. *Consider a swarm consisting of N agents with dynamics and control input in (3.1)-(3.2) and a leader agent with dynamics as in Assumption 12. If Assumptions 8-13 are satisfied for the swarm and the leader, then as $t \to \infty$ the swarm centroid asymptotically approaches the hyperball around the leader with radius*

$$\|\overline{x} - x_L\| < \frac{F^r tr(\overline{\Lambda}) + F_L^r \sum_{i=1}^{N} \overline{\nu}_{L,i}}{N \underline{\underline{\omega}}_L}. \tag{3.5}$$

Proof. Consider the positive scalar function $V = \frac{1}{2}\tilde{e}^T\tilde{e}$. Then, $\dot{V} = \dot{\tilde{e}}^T\tilde{e} = \dot{\overline{x}}^T\tilde{e}$. Applying Proposition 3.2 and taking Assumption 8 into consideration, one obtains

$$\dot{V} = \frac{1}{N}\sum_{i=1}^{N}\sum_{j=1,j\neq i}^{N} \nu_{ij} g^r(\|x_i - x_j\|)(x_i - x_j)^T\tilde{e}$$
$$+ \frac{1}{N}\sum_{i=1}^{N} \nu_{L,i}\ g_L^r(\|x_i - x_L\|)(x_i - x_L)^T\tilde{e} - \frac{1}{N}\sum_{i=1}^{N} w_{L,i}(x_i - x_L)^T\tilde{e},$$

$$\leq \frac{F^r}{N}\|\tilde{e}\|\sum_{i=1}^{N}\sum_{j=1,j\neq i}^{N}\nu_{ij} + \frac{F_L^r}{N}\|\tilde{e}\|\sum_{i=1}^{N}\nu_{L,i} - \frac{1}{N}\sum_{i=1}^{N}w_{L,i}(x_i - x_L)^T\tilde{e}.$$

Notice that by Assumption 13,

$$\sum_{i=1}^{N}w_{L,i}(x_i - x_L)^T\tilde{e} = \omega_L\tilde{e}^T\sum_{i=1}^{N}(x_i - x_L) = \omega_L\tilde{e}^T N\tilde{e},$$

and

$$\sum_{i=1}^{N}\sum_{j=1}^{N}\nu_{ij} \leq tr(\overline{\Lambda}),$$

therefore

$$\dot{V} \leq \|\tilde{e}\|\left[\frac{F^r}{N}tr(\overline{\Lambda}) + \frac{F_L^r}{N}\sum_{i=1}^{N}\overline{\nu}_{L,i} - \underline{\underline{\omega}}_L\|\tilde{e}\|\right].$$

Since $\|\tilde{e}\| = \sqrt{2V}$, we have $\dot{V} < 0$ when

$$\frac{F^r tr(\overline{\Lambda}) + F_L^r\sum_{i=1}^{N}\overline{\nu}_{L,i}}{\sqrt{2}N\underline{\underline{\omega}}_L} < \sqrt{V},$$

and therefore the swarm centroid will globally and exponentially converge to a hyperball around the leader with radius in (3.5). □

3.2.4 Ultimate swarm size

In [38], it is shown that under general communication topology and fixed coupling weights, the trajectories of the swarm converge to a hyperellipsoid centered at the weighted center of the swarm. Let $\xi = [\xi_1\ \xi_2\ ...\ \xi_N]$ be the left eigenvector of a coupling matrix W corresponding to the zero eigenvalue. The weighted center is defined as

$$\tilde{x} = \sum_{i=1}^{N}\xi_i x_i,$$

where, without loss of generality, the weights are assumed to be such that $\sum_{i=1}^{N}\xi_i = 1$. In light of Lemma 2.2, for any balanced coupling topology $\xi = \frac{1}{N}[1\ 1\ ...\ 1]^T$, and therefore the weighted center and the swarm centroid overlap. In addition, as long as $W(t)$ is balanced, $\xi(t) = \frac{1}{N}[1\ 1\ ...\ 1]^T$.

The eigenvalues of the irreducible and symmetric matrix $W^*(t) = \frac{1}{N}(W(t) + W^T(t))$ can be enumerated as

$$0 = \mu_1(t) > \mu_2(t) \geq \mu_3(t) \geq ... \geq \mu_N(t).$$

Furthermore, let $\mu(t)$ without any subscript denote the second largest eigenvalue, that is $\mu(t) = \mu_2(t) < 0$. Notice, that $-\mu(t)$ is the algebraic connectivity of the connected graph G^* for which $L(G^*) = -W^*(t)$ is its Laplacian. Moreover, let $\underline{\mu}$ be the second largest eigenvalue of $\underline{W^*} = \frac{1}{N}(\underline{W} + \underline{W^T})$.

Proposition 3.5. *Consider a swarm consisting of N agents with dynamics and control input in (3.1)-(3.2), and a leader agent with dynamics as in Assumption 12. If Assumptions 8-13 are satisfied for the swarm and the leader, then as $t \to \infty$ all follower agents asymptotically approach the swarm centroid such that*

$$\sum_{i=1}^{N} \|x_i - \overline{x}\|^2 \leq \epsilon^2, \tag{3.6}$$

where

$$\epsilon = \frac{F^r\sqrt{tr(\overline{\Lambda}^2)} + F_L^r\|\overline{K}_L\|}{-\frac{N}{2}\underline{\mu} + \underline{\underline{\omega}}}. \tag{3.7}$$

Proof. Let $e_i = x_i - \overline{x}$ and consider the positive definite function $V_i = \frac{1}{2}\frac{1}{N}e_i^T e_i$ for $i = 1, 2, ..., N$. Then we have $\dot{V}_i = \frac{1}{M}\dot{x}_i^T e_i - \frac{1}{M}\dot{\overline{x}}^T e_i$. Now define the positive definite function $V = \sum_{i=1}^{N} V_i$. Note that

$$\sum_{i=1}^{N} \dot{\overline{x}}^T e_i = \dot{\overline{x}}^T \sum_{i=1}^{N} e_i = 0,$$
$$x_i - x_j = e_i - e_j,$$
$$x_i - x_L = e_i + \tilde{e}.$$

In light of Assumption 8 we obtain

$$\begin{aligned}
\dot{V} =& \sum_{i=1}^{N} \dot{V}_i = \frac{1}{N}\sum_{i=1}^{N} \dot{x}_i^T e_i - \frac{1}{N}\sum_{i=1}^{N} \dot{\overline{x}}^T e_i, \\
=& -\frac{1}{N}\sum_{i=1}^{N}\sum_{j=1}^{N} w_{ij}(x_i - x_j)^T e_i + \frac{1}{N}\sum_{i=1}^{N}\sum_{j=1}^{N} \nu_{ij} g^r(\|x_i - x_j\|)(x_i - x_j)^T e_i \\
& - \frac{1}{N}\sum_{i=1}^{N} w_{L,i}(x_i - x_L)^T e_i + \frac{1}{N}\sum_{i=1}^{N} \nu_{L,i}\, g_L^r(\|x_i - x_L\|)(x_i - x_L)^T e_i,
\end{aligned}$$

$$\leq -\frac{1}{N}\sum_{i=1}^{N}\sum_{j=1}^{N} w_{ij}(e_i - e_j)^T e_i + \frac{1}{N}F^r \sum_{i=1}^{N}\|e_i\| \sum_{j=1, j\neq i}^{N} \nu_{ij} - \frac{1}{N}\sum_{i=1}^{N} w_{L,i} e_i^T e_i$$
$$- \frac{1}{N}\sum_{i=1}^{N} w_{L,i}\tilde{e}^T e_i + \frac{1}{N}F_L^r \sum_{i=1}^{N}\nu_{L,i}\|e_i\|. \tag{3.8}$$

Denote $e = \begin{bmatrix} e_1^T & e_2^T & ... & e_N^T \end{bmatrix}^T \in \mathbb{R}^{Nn}$. In the following the inequality

$$\sum_{i=1}^{N} a_i b_i \leq \sqrt{\sum_{i=1}^{N} a_i^2}\sqrt{\sum_{i=1}^{N} b_i^2}, \quad a_i, b_i \geq 0, i, j = 1, 2, ..., N$$

will be used. First notice that

$$\sum_{i=1}^{N} w_{L,i}\tilde{e}^T e_i = \omega_L \tilde{e}^T \sum_{i=1}^{N} e_i = 0,$$

and

$$-\sum_{i=1}^{N}\sum_{j=1}^{N} w_{ij}(e_i - e_j)^T e_i = \sum_{i=1}^{N}\sum_{j=1}^{N} w_{ij} e_j^T e_i - \sum_{i=1}^{N} e_i^T e_i \sum_{j=1}^{N} w_{ij} = \sum_{i=1}^{N}\sum_{j=1}^{N} w_{ij} e_j^T e_i. \tag{3.9}$$

For the other terms in (3.8), we have

$$\sum_{i=1}^{N} \nu_{L,i}\|e_i\| \leq \|\overline{K}_L\|\|e\|,$$
$$\sum_{i=1}^{N}\|e_i\| \sum_{j=1, j\neq i}^{N} \nu_{ij} \leq \|e\| \sqrt{\sum_{i=1}^{N}\sum_{j=1, j\neq i}^{N} \nu_{ij}^2} \leq \sqrt{tr(\overline{\Lambda}^2)}\|e\|,$$
$$-\sum_{i=1}^{N} w_{L,i} e_i^T e_i \leq -\underline{\omega}\|e\|^2.$$

It is shown in [38] that for constant W and μ

$$\frac{1}{N}\sum_{i=1}^{N}\sum_{j=1}^{N} w_{ij} e_j^T e_i = \frac{1}{2} e^T \left[\frac{1}{N}(W + W^T) \otimes I_n\right] e$$
$$\leq \mu\|e\|^2.$$

In our case $W = W(t)$ and $\mu = \mu(t)$. Let G^* be the weighted undirected graph on N vertices, which has the graph Laplacian $L(G^*) = -\frac{1}{N}(W + W^T)$. Since $W + W^T$ is irreducible (see

Lemma 2.2), G^* is connected, with Laplacian eigenvalues

$$0 = \lambda_1^*(t) < \lambda_2^*(t) \leq \lambda_3^*(t) \leq ... \leq \lambda_N^*(t).$$

Then,

$$\lambda_1^*(t) = -\mu_1(t), \lambda_2^*(t) = -\mu_2(t), ..., \lambda_N^*(t) = -\mu_N(t).$$

In light of Lemma 2.3, the minimum of $\lambda_2^*(t)$ is obtained if $W(t) = \underline{W}$, denoted by $\underline{\lambda}_2^*$. Increasing any edge-weights may only increase the algebraic connectivity of the graph. Therefore $\lambda_2^*(t) \geq \underline{\lambda}_2^*$ for all $t > 0$. Consequently,

$$\mu(t) = \mu_2(t) = -\lambda_2^*(t) \leq -\underline{\lambda}_2^* = \underline{\mu},$$

and

$$\frac{1}{N}\sum_{i=1}^{N}\sum_{j=1}^{N} w_{ij} e_j^T e_i \leq \frac{1}{2}\underline{\mu}\|e\|^2 < 0.$$

Combining the results for each term of (3.8), we obtain

$$\dot{V} \leq \|e\|\left[(\frac{1}{2}\underline{\mu} - \frac{1}{N}\underline{\underline{\omega}})\|e\| + \frac{1}{N}F^r\sqrt{tr(\overline{\Lambda}^2)} + \frac{1}{N}F_L^r\|\overline{W}_L\|\right].$$

Since $\|e\| = \sqrt{2NV}$, when

$$\sqrt{V} > \frac{\frac{1}{N}F^r\sqrt{tr(\overline{\Lambda}^2)} + \frac{1}{N}F_L^r\|\overline{W}_L\|}{\sqrt{2N}(\frac{1}{2}\underline{\mu} - \frac{1}{N}\underline{\underline{\omega}})}$$

we have $\dot{V} < 0$ and the swarm will globally and exponentially converge to the hyperellipsoid described in (3.6) and (3.7).

□

Remark 3.6. In [42] fully connected and symmetric attraction and repulsion graphs with equal weights are assumed. That is, for N followers

$$W = k^a(t)\begin{bmatrix} -(N-1) & 1 & ... & 1 \\ 1 & -(N-1) & ... & 1 \\ 1 & 1 & ... & 1 \\ 1 & 1 & ... & -(N-1) \end{bmatrix},$$

where $k^a(t)$ denotes the inter-agent attraction weight at time t, such that $0 < \underline{k}^a \leq k^a(t) \leq \overline{k}^a \quad \forall t > 0$. Similarly, the leader attraction is equal for each agent such that $0 < \underline{k}^a_L \leq k^a_L(t) \leq \overline{k}^a_L \quad \forall t > 0$. The algebraic connectivity of a simple, complete graph K_n on n vertices is n [53]. Notice, that

$$W(t) = -k^a(t)\ L(K_n).$$

Therefore, due to the symmetry of W we have

$$\underline{\mu} = -\frac{2}{N}\underline{k}^a N = -2\underline{k}^a.$$

From here, it is straightforward to show, that

$$\epsilon = \frac{F^r(N-1)\sqrt{(N)} + F^r_L\sqrt{(N)}}{N\underline{k}^a + k^a_L},$$

which matches with the result in [42].

3.3 Applications in swarm coordination

3.3.1 Switching swarm topology

In Section 3.2, we investigated the swarm behavior with fixed, balanced communication topology and derived a bound on the swarm size. However, by introducing some assumptions, the same results may be applied to time-varying swarm topologies.

Consider the framework discussed in the previous section, and a swarm of N followers and a leader with symmetric coupling. Let $G_{a,f}(V, E_{a,f}, A_{a,f})$ denote the *fixed attraction graph* on $N+1$ vertices (including the leader), which is the time-invariant component of the attraction graph and assumed to be connected.

Let W denote the attraction coupling matrix of the fixed attraction graph, and W' denote the attraction coupling matrix of the graph obtained from $G_{a,f}$ by inserting a new undirected edge with weight as in Assumption 10. Let μ' denote the second largest eigenvalue of the irreducible matrix $\frac{1}{N}(W' + W'^T)$. In light of Lemma 2.3, inserting a new edge into $G_{a,f}$ may only increase its algebraic connectivity. Consequently, $\mu'(t) \leq \mu(t) \leq \underline{\mu}$ must hold for all t. Naturally, the inequality will hold for subsequent inserted edges as well. In other words, inserting a new attraction link into the swarm topology may only decrease the ultimate bound on the swarm size.

Let $G_{r,c}(V, E_{r,c}, A_{r,c})$ denote the *complete repulsion graph*, where repulsion acts between any two agents, and the repulsion coupling weights satisfy Assumption 10. It is straightforward to see, that the ultimate swarm size from Proposition 3.5 may only decrease by removing any repulsion links from the swarm topology.

Let $\epsilon(G_a, G_r)$ denote the ultimate swarm size of the swarm with attraction graph G_a and repulsion graph G_r. Let G_a^+ denote any attraction graph obtained by inserting edges into $G_{a,f}$, and G_r^- denote any repulsion graph obtained by removing edges from $G_{r,c}$. Then we can state that $\epsilon(G_a^+, G_r^-) < \epsilon(G_{a,f}, G_{r,c})$. Therefore, if we assume that the edges of the fixed attraction topology are maintained for all t, by determining $\epsilon(G_{a,f}, G_{r,c})$, we obtain a conservative upper bound on the ultimate swarm size with changing attraction and repulsion topology.

3.3.2 Limiting distance between agents

In certain applications it is desirable to limit the maximum distance between any two agents in order to maintain swarm cohesion and communication. This can be achieved by adjusting the attraction coupling between agents getting out of range from each other.

Assume, that we want to limit the distance between agents i and j so that $\|x_i - x_j\| \leq R_{i,j}$, where $R_{i,j} > 0$ is the *critical distance* between agent i and j and the initial inter-agent distance is less than $R_{i,j}$. An approach to achieve it is to set ω_{ij} so that

$$\frac{1}{2}\frac{d}{dt}(x_i - x_j)^T(x_i - x_j) < 0,$$

whenever $\|x_i - x_j\| \geq R_{i,j}$. For the sake of simplicity, we will further assume that the velocity vector $\dot{x}_j = v_j$ of agent j is available for agent i. Then, we have

$$\begin{aligned}
&\frac{1}{2}\frac{d}{dt}(x_i - x_j)^T(x_i - x_j) = \\
=&(\dot{x}_i - \dot{x}_j)^T(x_i - x_j) - \sum_{k=1,k\neq i,j}^{N} w_{ik}(x_i - x_k)^T(x_i - x_j) \\
&+ \sum_{k=1,k\neq i}^{N} \nu_{ik}\, g^r(\|x_i - x_k\|)(x_i - x_k)^T(x_i - x_j) - w_{L,i}(x_i - x_L)^T(x_i - x_j) \\
&+ \nu_{L,i}\, g_L^r(\|x_i - x_L\|)(x_i - x_L)^T(x_i - x_j) - v_j(x_i - x_j) - w_{ij}\|x_i - x_j\|^2, \\
=&H(x)(x_i - x_j) - w_{ij}\|x_i - x_j\|^2 < 0.
\end{aligned}$$

Therefore, if we choose w_{ij} such that

$$\frac{H(x)(x_i - x_j)}{\|x_i - x_j\|^2} < w_{ij}, \tag{3.10}$$

then

$$\frac{1}{2}\frac{d}{dt}\|x_i - x_j\|^2 < 0$$

is satisfied.

To implement the attraction weights for limited interagent distance, agent i must check its distance from agent j. In the case when $\|x_i - x_j\| \geq R_{i,j}$, w_{ij} is switched according to (3.10). A formula can be derived using the same approach if the other agent's velocity vector is unknown to agent i.

3.4 Simulation

In this section we will verify our results through numerical simulations. Consider a swarm with $N = 6$ follower agents and a leader. The states evolve in $\mathbb{R}^2$ governed by (3.1), where the attraction and repulsion functions have the following forms:

$$\begin{aligned}
f^a_{i,j} &= w_{i,j}(t)(x_i - x_j), \\
f^r_{i,j} &= \nu_{i,j}(t)e^{-\frac{\|x_i - x_j\|^2}{r}}(x_i - x_j), \\
f^a_{L,i} &= w_{L,i}(t)(x_i - x_L), \\
f^r_{L,i} &= \nu_{L,i}(t)e^{-\frac{\|x_i - x_L\|^2}{r_L}}(x_i - x_L),
\end{aligned}$$

where r and r_L are scalars, and chosen to be $r = r_L = 2$. It is straightforward to see that $F^r = \sqrt{\frac{r}{2e}}$, and $F^r_L = \sqrt{\frac{r_L}{2e}}$.

3.4.1 Swarm size adjustment

Adjusting the swarm size of robotic swarms may be necessary in order to move through terrains with obstacles. In this simulation the focus is on the coordination of the follower agents, therefore we will omit the leader. First, we let the swarm to approach an equilibrium state with the weights $w_{ij} = 2$ and $\nu_{ij} = 5$ for each edge in the graph in Fig. 3.1. Then, the weights are switched to $w_{ij} = 4.5$ and $\nu_{ij} = 4.8$ for each edge.

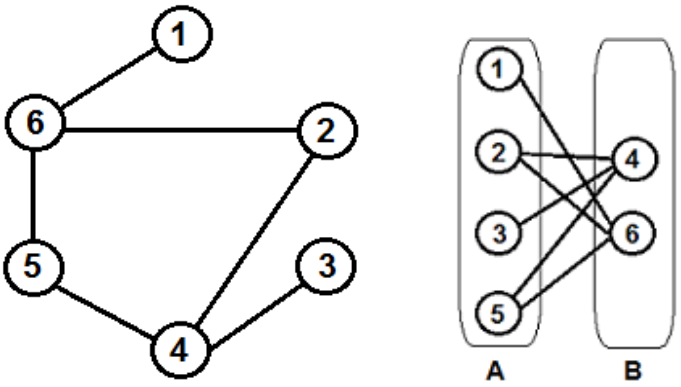

(a) Topology representing both the attraction and repulsion graph

(b) Partitioning of the same graph into two disjoint sets

Figure 3.1: Graph G representing the interaction topology used throughout the simulation cases

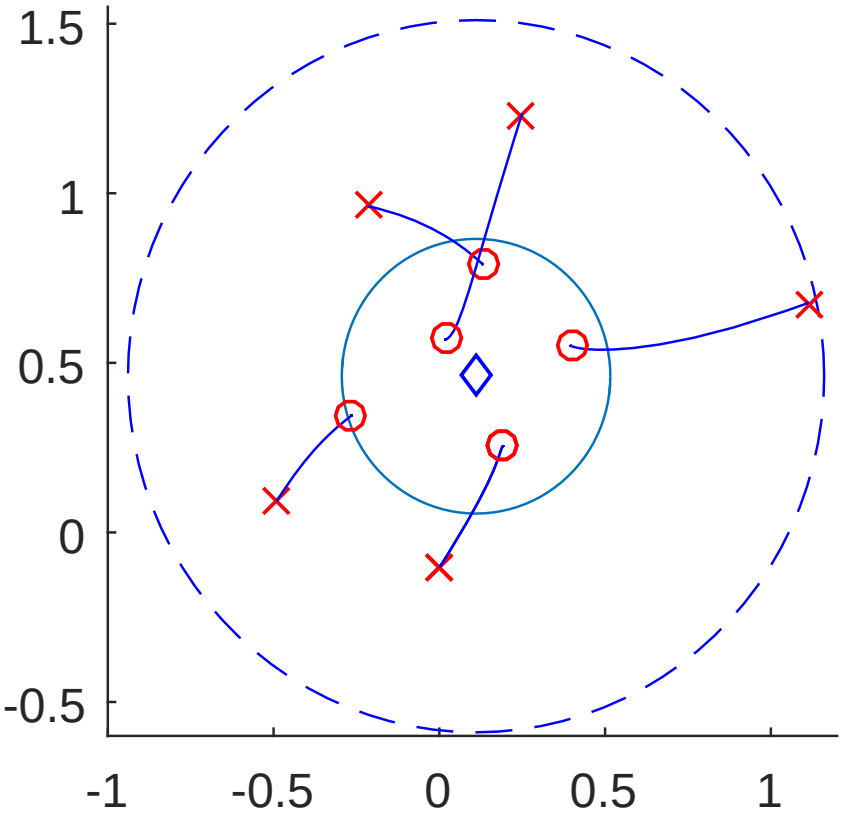

Figure 3.2: Simulation 1: Approximate swarm size before (dashed line) and after (solid line) switching attraction and repulsion weights. The swarm centroid is indicated by the diamond marker.

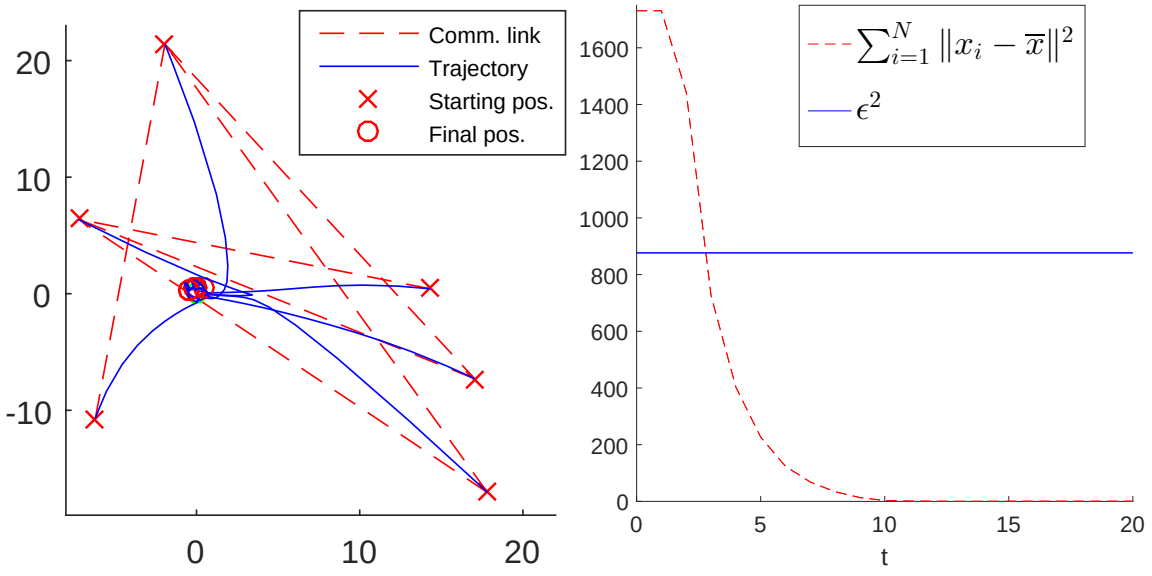

(a) Complete agent trajectories

(b) Agent-centroid squared error

Figure 3.3: Simulation 2: Agent-centroid squared error converges to the region derived in Proposition 3.5

The results can be observed in Fig. 3.2, where the concentric circles are estimates of the swarm size before and after the switching. Note, that the swarm centroid is immobile, because the coupling is symmetric and no leader is present.

3.4.2 Ultimate swarm size with time-varying weights

In this numerical example, we compare the ultimate swarm size obtained in Proposition 3.5, to the simulated size of the swarm while the coupling weights are allowed to change within some predefined bounds. The coupling weights were sinusoidal functions, such that $\underline{w}_{ij} = \underline{\omega}_L = 1, \quad \overline{w}_{ij} = \overline{\omega}_L = 9, \underline{\nu}_{ij} = \underline{\nu}_{L,i} = 2, \quad \overline{\nu}_{ij} = \overline{\nu}_{L,i} = 10$, for i, j pairs which are connected by an edge of the communication graph in Fig. 3.1.

The simulation results are presented in Fig. 3.3. The agents approach the leader at the origin (Fig. 3.3(a)), and remain in its vicinity. The system state converges to and remain within the hyperellipsoid described in Proposition 3.5.

3.4.3 Collision avoidance

Collision avoidance is an important property of distributed control algorithms. Applying the reasoning in Section 3.3.1, let the fixed swarm interactions be represented by graph $G(V, E)$ in

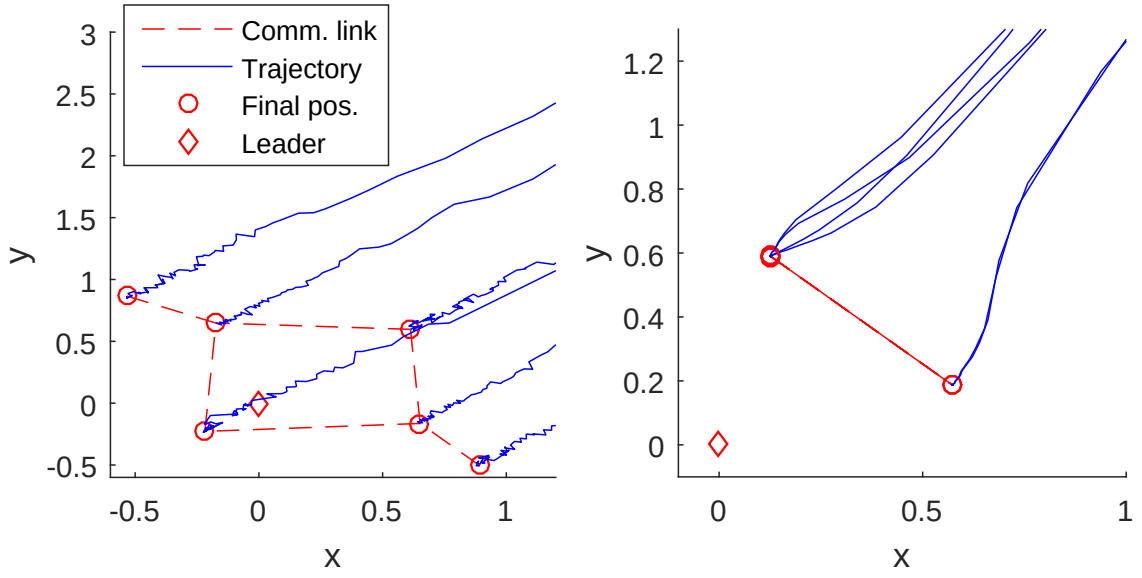

(a) Aggregation with collision avoidance

(b) No collision avoidance: agents not connected cannot avoid collision

Figure 3.4: Simulation 3: Agent trajectories with and without collision avoidance

Fig. 3.1 (both attraction graph G^a and repulsion graph G^r). Whenever disconnected agents i and j approach each other within $R^c_{ij} \in \mathbb{R}^+$ critical distance, insert a new edge e into G^r between agent i and j. As they leave each other's neighborhood of radius R^c_{ij}, remove edge e.

Let ν_c denote the weight of the inserted repulsion edge. In this simulation, we let the critical distance take the form

$$R^c_{ij} = \sqrt{r \cdot \frac{\nu_c}{w_{ij}}} + \varepsilon,$$

the values were empirically set to $\nu_c = 6, \varepsilon = 0.5$. For the sake of simplicity, we choose the fixed coupling weights as

$$w_{ij} = 5, \quad \nu_{ij} = 6, \quad \forall \{i,j\} \in E,$$

$$w_{L,i} = 5, \quad \nu_{L,i} = 6 \quad \forall\, i,$$

for all $t > 0$.

The same simulation was repeated without applying the aforementioned collision avoidance technique. As Fig. 3.4(a) shows, by using collision avoidance, the agents aggregated around the leader, and all agents without fixed interaction link avoided collision. In Fig. 3.4(b) one may observe, that disconnected agents are organized in two groups and converge to two distinct points around the leader. The underlying reason is that G is bipartite, that is its vertices can be divided into two disjoint sets A and B such that every edge connects a vertex in A to a vertex

in B (Fig. 3.1(b)). Therefore, agents in the same set has no interaction with each other, and will eventually collide.

3.5 Conclusions

In this chapter, we have investigated the collective behavior of leader-follower swarms, where the interaction topology can be described by an attraction and a repulsion graph with time-varying weights. Centroid motion and leader-centroid distance was analyzed, then quantitative connection was established between the ultimate swarm size and the bounds on the time-varying weights using results from algebraic graph theory. We discussed applications of time-varying coupling weights and topologies in distributed control and presented numerical simulations to demonstrate our results. Agents of higher order dynamics and the influence of communication time-delays on the swarm size serves as future research topics.

Chapter 4

Experiments

4.1 Introduction

Experimental validation is an important aspect in the design of distributed control algorithms, but also a challenging one. First of all, selecting a robotic platform is a critical issue, which can make or break the experiment. For multi-agent system modeling the following considerations must be taken into account:

- Relatively small size: The size of the robots must be comparably small with respect to the allocated space for the experiment in order to observe the trajectories and the interaction between agents.
- Large number of robots: since we are aiming at modeling a multi-agent system the experiment will be designed for several (at least 5-6) robots. Therefore, it might be necessary to design for less complex, inexpensive platforms.
- Communication: the robots must be able to communicate with each other real-time, and also receive commands or information from external sources (such as a PC). The speed, bandwidth and latency of the communication channel are all important factors.
- Safety: implementing the desired algorithm properly for the first time is almost impossible, usually several iterations are necessary. This results in unexpected behavior, which may damage the robots, the environment or the operator. Therefore it is necessary to implement some safety measures in the experimental setup (both physically and in the software).

On top of these issues the agents' state must be fed back and made available to other agents. The most common case is to use position feedback, and therefore we need some means of obtaining that in real-time. Designing such an experimental setup is a complex issue and requires a comprehensive understanding of both the control aspect and general system engineering disciples. One major goal of the *Mechatronics and Controls Laboratory* is to set up a platform for testing and validating such distributed control algorithms as the ones proposed in this thesis. Although the main contribution of this thesis work is the introduced theoretical framework, the first steps of the aforementioned endeavor were realized as part of this work. The following goals were set forth:

- Set up communication with a quadcopter from a PC. The quadcopter is intended to model a single agent in the multi-agent system.
- Stabilize its position and attitude, since for the proposed control framework it is necessary to maintain the position with high accuracy.
- Be able to maneuver it between predefined waypoints using control commands sent from the PC.

The organization of the chapter is as follows: first the experimental setup and its fundamental components are introduced in Section 4.2. In Section 4.3 the designed controller for position and attitude stabilization is introduced. Lastly the future directions are outlined in Section 5.

4.2 Experimental setup

The experimental setup consists of the following components: a quadcopter, an area surrounded by protective net (referred to as the cage), a motion tracking camera system laid out around the cage, a PC connected to the camera system and a PC sending control commands to the quadcopter (see Fig. 4.1).

4.2.1 Quadcopter

The quadcopter is a *Hummingbird* model (see Fig. 4.2) from the company *AscTec*. This is a small and agile unmanned aerial vehicle designed for research purposes, in particular for swarming and controls experiments. Some technical data from the manufacturer's website [1]:

- Dimensions: 54 x 54 x 5.5 cm

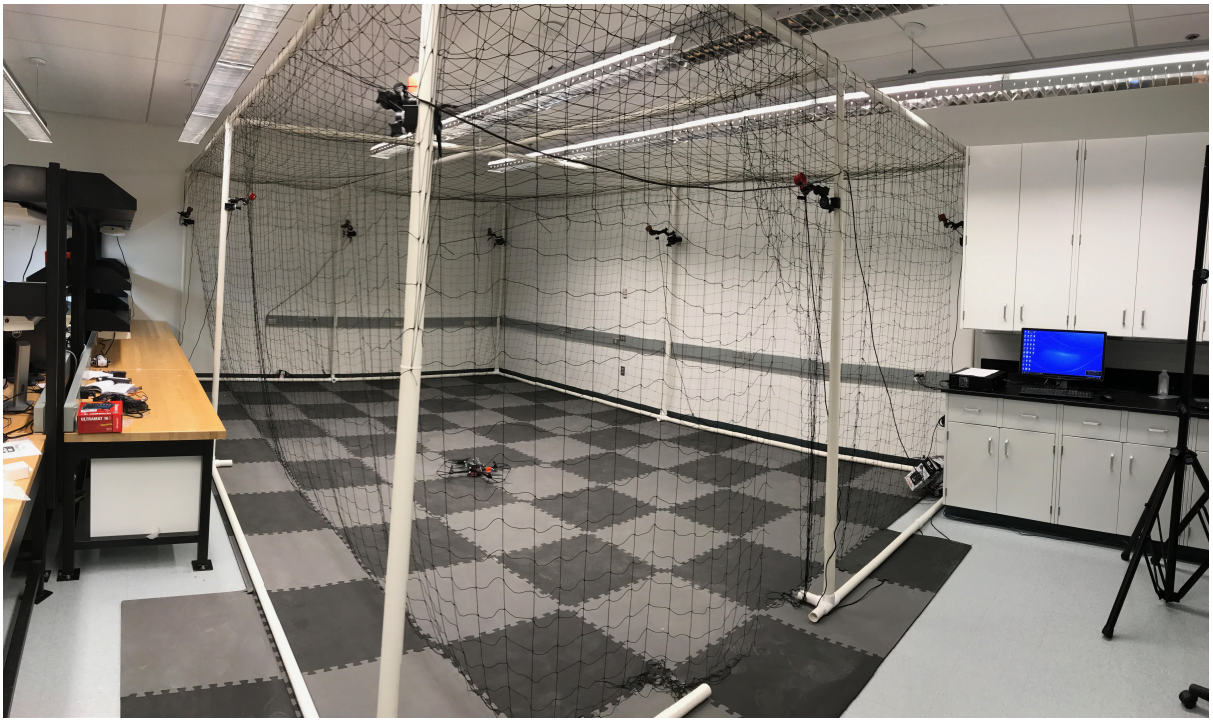

Figure 4.1: Experimental setup in the UNH Mechatronics and Controls Laboratory

- Propeller size: 8”
- Motors: 4 x 80 W
- Maximum thrust: 20 N
- Maximum payload: 200 g
- Maximum total weight: 710 g
- Maximum airspeed: 15 $\frac{m}{s}$
- Maximum flight time: 20 mins without payload
- Battery: 2100 mAh LiPo

Propeller protector is attached to the experimental model. A remote control (*Futaba T8J*) was provided with the quadcopter sending control signals through serial communication. The AscTec Hummingbird is equipped with an *Atomboard v3* onboard computer, with the following specifications [54]:

- CPU: Intel Atom Processor E3845

Figure 4.2: AscTec Hummingbird, the model used in the experiments [1]

- Number of cores: 4
- Clock speed: 1.91 GHz
- RAM: 4 GB DDR3
- Hard Disk: 64 GB SSD, 8 GB eMMC
- Network: Gigabit Ethernet
- USB: 5 x USB2.0, 1 x USB3.0

The model also comes with a pair of pre-configured XBee modules providing serial communication link between the quadcopter's onboard computer and another device to which the other XBee is connected.

The communication interface to the onboard computer's *Low Level Processor* (responsible for DC motor control) is specified in [55]. To summarize, we may send the following control commands: roll/pitch/yaw in degrees and thrust in % of maximum value. The onboard control algorithm, which directly controls the DC motor voltages to track the control command signal

is closed source. First, the serial programming interface must be enabled via the remote control in order to allow the quadcopter to accept control commands from other sources. It is important to mention that the control command must be sent with at least $10Hz$ frequency, otherwise the quadcopter switches to autopilot mode.

Moreover, the interface provides access to the quadcopter's onboard sensor data, such as the accelerometers or gyroscope in the form of polling. A polling request package must be sent in which the requested data is specified. The onboard processor assembles a package with the required data and sends it back to the requester. However, there are serious issues with this method when it comes to implementing real-time control algorithms. Most importantly, the real-time operation is not guaranteed. There is no guaranteed time in which we receive the requested data package for feedback. Secondly, alternating between control command packages, polling packages and receiving the polling data in real-time leads to a complicated multi-threaded software solution. Lastly, the onboard sensor data proved to be too noisy for precise control applications, and therefore a more accurate position and velocity feedback method was required in the form of a motion tracking camera system.

4.2.2 Motion tracking camera system

To provide high-precision position feedback, a system of motion tracking cameras were utilized around the cage. Eight cameras were used evenly distributed along the walls of the cage (Fig. 4.3). The cameras were set up so that they point to the middle of the space enclosed by the protective net. The camera model used is the *Flex 13* from the company Optitrack, with the following specifications[56]:

- Dimensions: 53.8 x 81 x 42.4 mm
- Weight: 186 g
- Lens: 5.5 mm focal length at f/1.8, with 800nm IR long pass filter
- Horizontal/Vertical FOV: 56°/46°
- Resolution: 1280 x 1024
- Frame rate: 30-120 FPS

The software *Optitrack Motive* is provided by the manufacturer providing calibration support and easy access to tracking data as well as streaming options. After setup, the cameras must

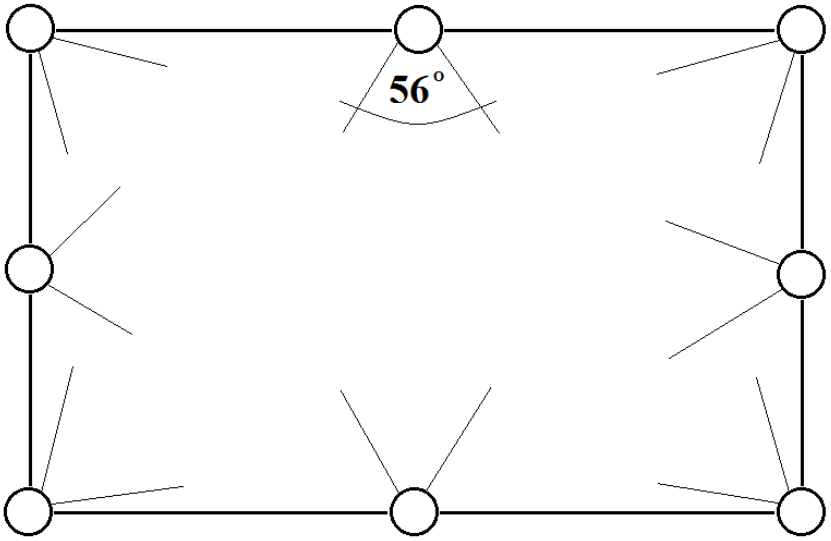

Figure 4.3: Layout of motion tracking cameras

be calibrated using a calibration wand and a calibration frame. The resulting mean error of position measurement according to Motive is around $0.5mm$.

The camera system is capable of detecting and tracking IR (infrared) markers. In Motive markers can be grouped to form a rigid body, both the position and orientation of rigid bodies can be tracked in real-time. Fig. 4.4 shows the markers attached to the quadcopter, added as a rigid body in Motive.

Motive can be set up to stream rigid body data real-time across networks. The streamed data consists of the position of the individual markers as well as the orientation of the rigid body represented by quaternions. The position of the rigid body's pivot is also streamed, which will be used to represent the quadcopter location in the experiments. The pivot is the center-of-mass of the markers constituting the rigid body. The stream can be accessed by a remote computer, on which the quadcopter control algorithm is running.

4.3 Controller design

Even though attitude and height control is implemented on the quadcopter's onboard computer (closed source), due to the inaccuracy of its sensors a significant drift can be observed right after take off, with the reference roll/pitch/yaw degrees all being zero. The drift can be compensated to a certain degree using the remote control's trimming option (setting a constant bias to the roll/pitch/yaw commands), but it is far from satisfactory for distributed control purposes.

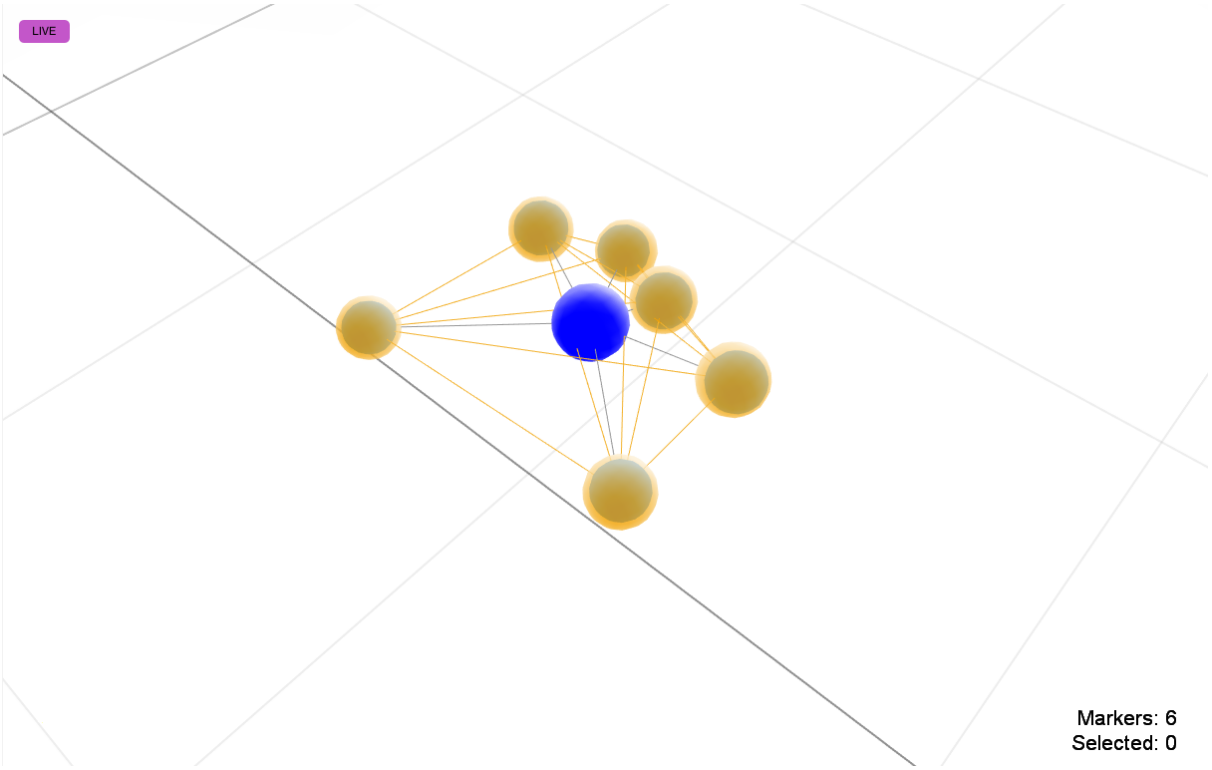

Figure 4.4: Rigid body representing the quadcopter as seen in Motive (inverted colors). Yellow balls represent the actual markers in 3D space, the blue sphere indicates the marker pivot.

Instead of using the quadcopter's noisy sensor data, the position feedback was used to stabilize the quadcopter's position.

A remote computer in the laboratory is set up to receive the real-time streaming data from Motive. The position provided by the camera system is with respect to the camera system's fixed frame of reference set up during calibration and referred to as *world frame*. Using the position of the rigid body from two consecutive camera frames, the velocity vector of the quadcopter can be determined in the world frame.

Due to the fact that only roll/pitch/yaw commands can be issued to the quadcopter (representing rotation about the $x-y-z$ axes of the quadcopter itself), the velocity vector must be transformed to *quadcopter frame*, that is it has to be represented in a coordinate frame fixed to the quadcopter. The transformation matrix can be determined based on the quaternion data streamed through the network (must be converted to Euler-angles first). The process described in [57] was implemented.

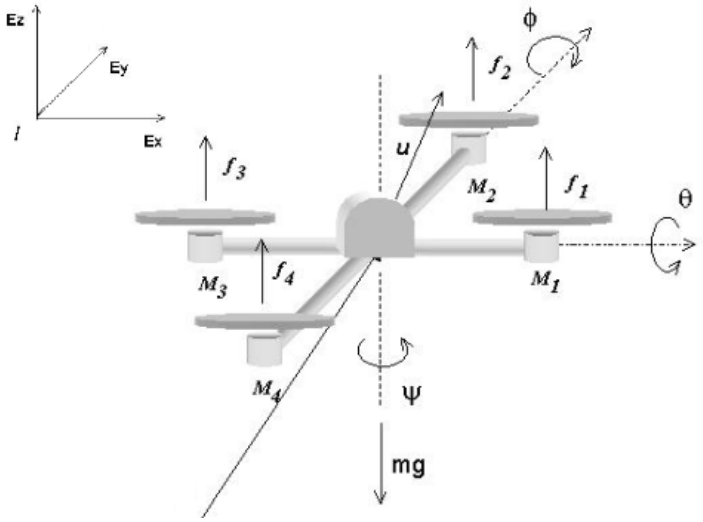

Figure 4.5: Free-body diagram and reference frame of the quadcopter model[2]

The second-order dynamic model of a quadcopter can be found in [2]. Using the notations as it can be observed in Fig. 4.5, the dynamic model takes the form

$$m\ddot{x} = -usin(\theta) \tag{4.1}$$

$$m\ddot{y} = ucos(\theta)sin(\phi) \tag{4.2}$$

$$m\ddot{z} = ucos(\theta)cos(\phi) - mg \tag{4.3}$$

$$\ddot{\psi} = \tilde{\tau_\psi} \tag{4.4}$$

$$\ddot{\theta} = \tilde{\tau_\theta} \tag{4.5}$$

$$\ddot{\phi} = \tilde{\tau_\phi}, \tag{4.6}$$

where $u = f_1 + f_2 + f_3 + f_4$ and $f_i = k_i\omega_i$, $k_i > 0$, ω_i is the angular speed of motor i; $\tilde{\tau_\psi}$, $\tilde{\tau_\theta}$ and $\tilde{\tau_\phi}$ are transformed angular moments (see [2] for more details).

Advanced nonlinear control techniques such as sliding mode control or adaptive control can be deployed to stabilize the quadcopter dynamics. However the main goal for this work was to implement a simple controller as a first step, which successfully stabilizes the nonlinear quadcopter dynamics. PID (proportional-integral-derivative) control is the most commonly used method providing acceptable results even without knowing the exact plant dynamics. In this project, separate PID control loops were designed for the x and y components of the velocity vector in the quadcopter's frame. It was assumed that the x component of the velocity vector $v_x = \dot{x}$ is proportional to the pitch, while the y component $v_y = \dot{y}$ is proportional to the roll. As a first approach, the component in z direction $v_z = \dot{z}$ pointing up can vary and it is controlled

through the thrust from the PC by the operator. The error signal for the PID controller is formulated as $e_x = v_{rx} - v_x$ and $e_y = v_{ry} - v_y$. For lateral position stabilization the reference velocity for both components $v_{rx} = v_{ry} = 0$.

The PID controller gains were tuned empirically, and selected as follows:

$$K_P^x = K_P^y = 6,\ K_I^x = K_I^y = 0.4,\ K_D^x = K_D^y = 1.$$

The output of the PID controller must be scaled and saturation must be applied to match the control command range as interpreted by the quadcopter, that is:

- Roll/pitch: integer in the range $[-2047, +2047]$ corresponding to -52° to +52°
- Thrust: integer in the range $[0, +4095]$ corresponding to 0% to 100% thrust

The designed controller was capable of stabilizing the quadcopter velocity in the x and y directions. However, the coupling between roll, pitch and thrust cannot be neglected. The oscillation in z direction increases with higher thrust value and minimal close to the ground (low thrust).

PID control loop was implemented for the z velocity component as well. The empirically tuned PID gains are

$$K_P^z = 2,\ K_I^z = 0.1,\ K_D^z = 1.$$

Using all three PID control loops the quadcopter position can be stabilized in a given height. However, the necessary PID gains for the thrust control depends on the thrust value and height about which we are trying to stabilize the position. The underlying reason for this is the quadcopter's nonlinear dynamics and the coupling between roll/pitch and thrust. Certain aerodynamic effects may take place when the quadcopter is close to the ground, which is out of the scope of the current study.

Fig. 4.6 shows the structure of the closed-loop system, where $u_v^{x/y/z}$ denotes the PID controller output and the actual control command value sent to the quadcopter is denoted by $u_{p/r/t}$ referring to pitch, roll and thrust respectively. Distinct PID control loops are implemented for the x, y and z components of the velocity vector reflected by the index/superscript $x/y/z$.

Furthermore, basic waypoint navigation has been implemented. Measuring the quadcopter's current position and knowledge of the predefined waypoint can be used to calculate the vector pointing from the quadcopter to the waypoint. This vector can be scaled and used as reference velocity for the PID controller. If the maximum reference velocity is small enough, the same PID gains can be used for waypoint navigation.

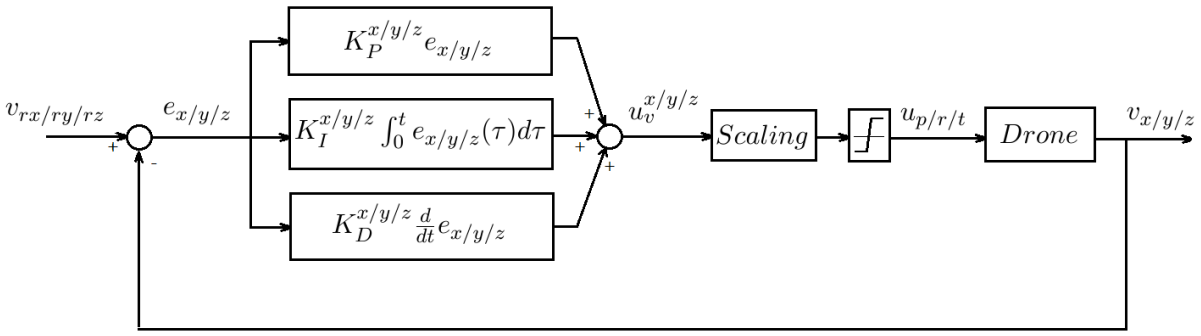

Figure 4.6: Closed-loop system with PID control (implemented as 3 distinct loops in x, y and z direction)

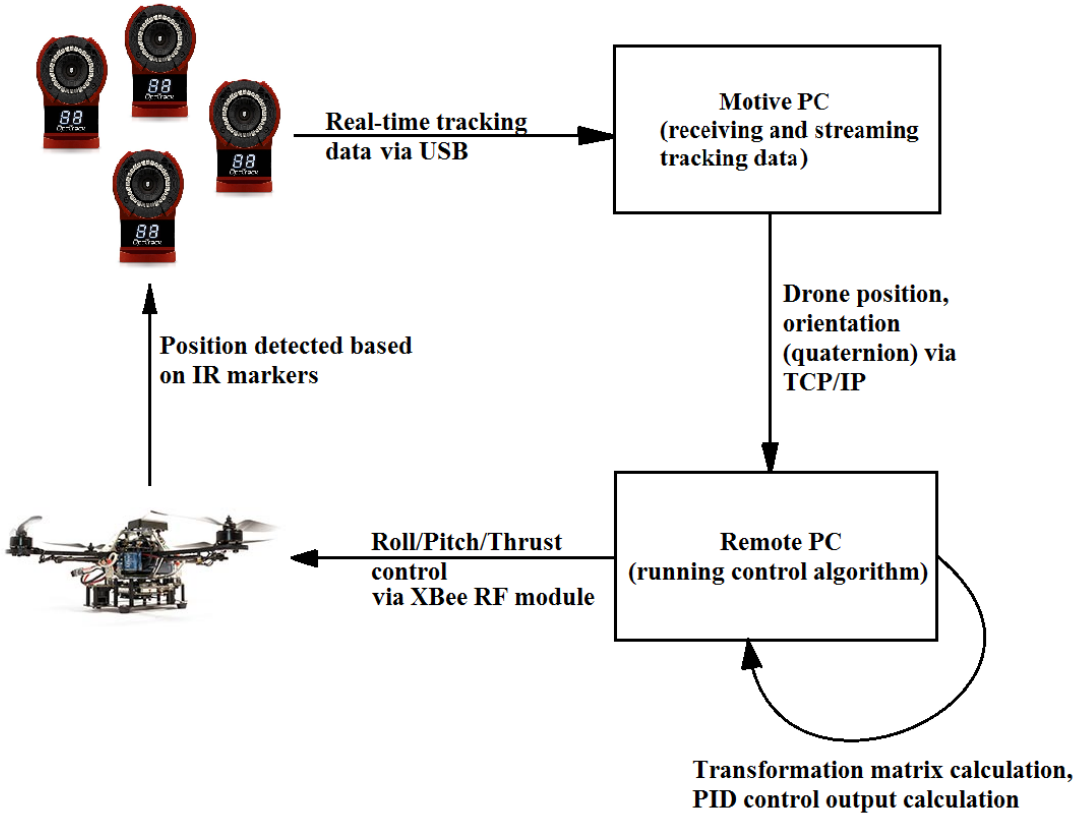

Figure 4.7: Sketch of the experimental setup including all components

The interconnection and function of the various components used in the experimental setup can be observed in Fig. 4.7.

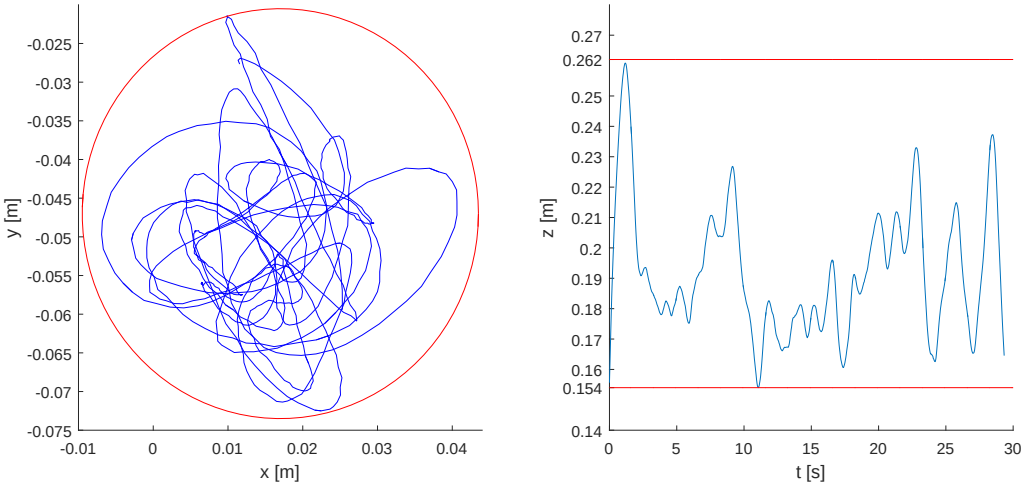

Figure 4.8: Position stabilization results using PID control. Quadcopter trajectory on the ground plane (left) can be confined into a circular area with radius $r = 2.65\ cm$ (red circle). Quadcopter altitude is oscillatory (right), the maximum distance between peaks is $d = 10.8\ cm$ (between red lines).

4.4 Experimental results

Experiments were performed to verify the stability and performance of the designed closed-loop system.

4.4.1 Position stabilization in ground plane

In the first experiment, position stabilization in the ground plane was tested. The thrust and therefore the altitude was adjustable from the remote PC. The quadcopter trajectory was recorded from starting position $(0.0253, \ -0.0594)$, which denotes the marker pivot's position (close to but not the same as the quadcopter's center of mass). As it has been mentioned in the previous section, verifying the position stabilization performance mainly means stabilization in the XY (ground) plane due to the effect of roll/pitch on the vertical velocity. Fig. 4.8 shows the obtained results. The position was stabilized within a bounded area with radius $r = 2.65\ cm$. The quadcopter altitude was oscillating with an amplitude of approximately $6cm$. These results might be further improved by fine-tuning the PID gains, however according to the experience of the author it is close to the limit of the applied control approach.

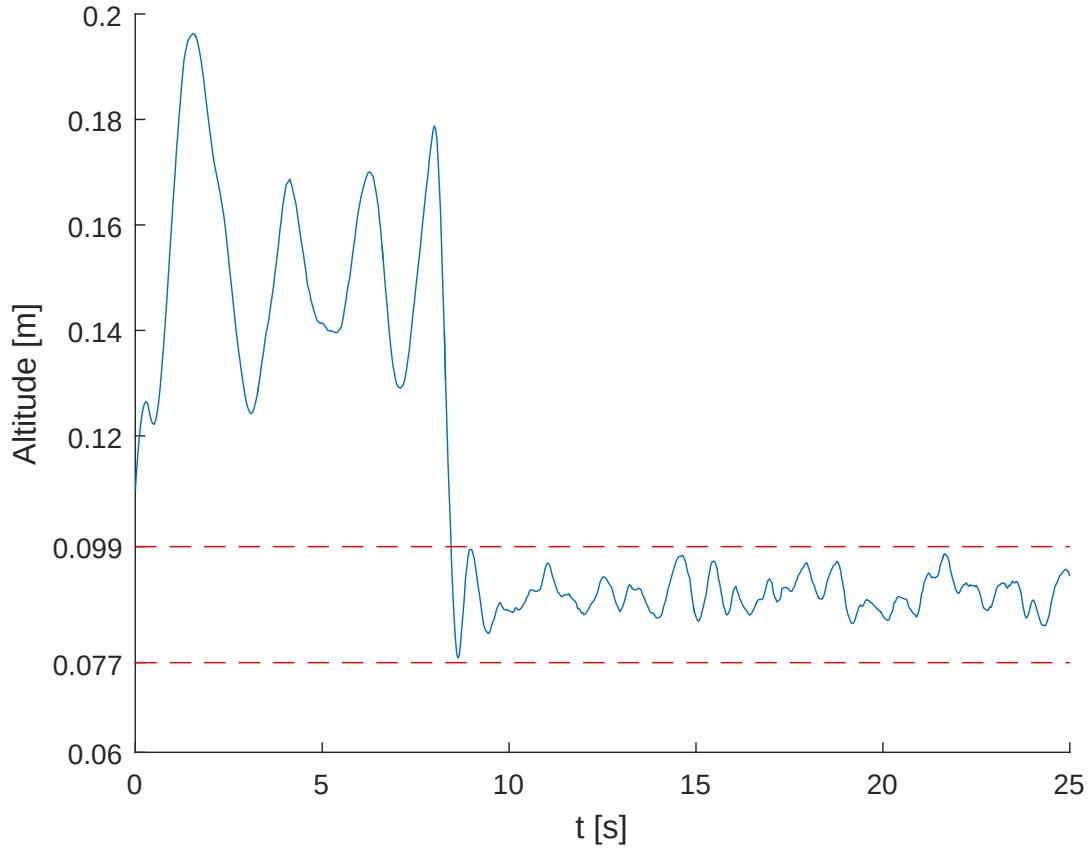

Figure 4.9: Altitude stabilization: Quadcopter altitude vs. time, the altitude stabilization is turned on at $t = 9\ s$. The altitude is stabilized through thrust control, the amplitude of oscillation in z-direction has been reduced to 1.1 cm as indicated by the red lines.

4.4.2 Position stabilization in fixed altitude

Stabilization of the vertical velocity can be achieved by using a third PID loop, where the output is v_z and thrust control command is sent to the quadcopter. However, due to the effect of roll/pitch on the vertical velocity (see Eq. 4.3) the appropriate PID gains strongly depend on the thrust value and therefore a different control technique would be more effective. The fixed control gains

$$K_P^z = 2,\ K_I^z = 0.1,\ K_D^z = 1$$

were used to stabilize the quadcopter altitude at a certain height. The results can be seen in Fig. 4.9 and 4.10. By introducing the third PID control loop, the amplitude of oscillation in z-direction is significantly lower (compare to Fig. 4.8), around 1.1 cm.

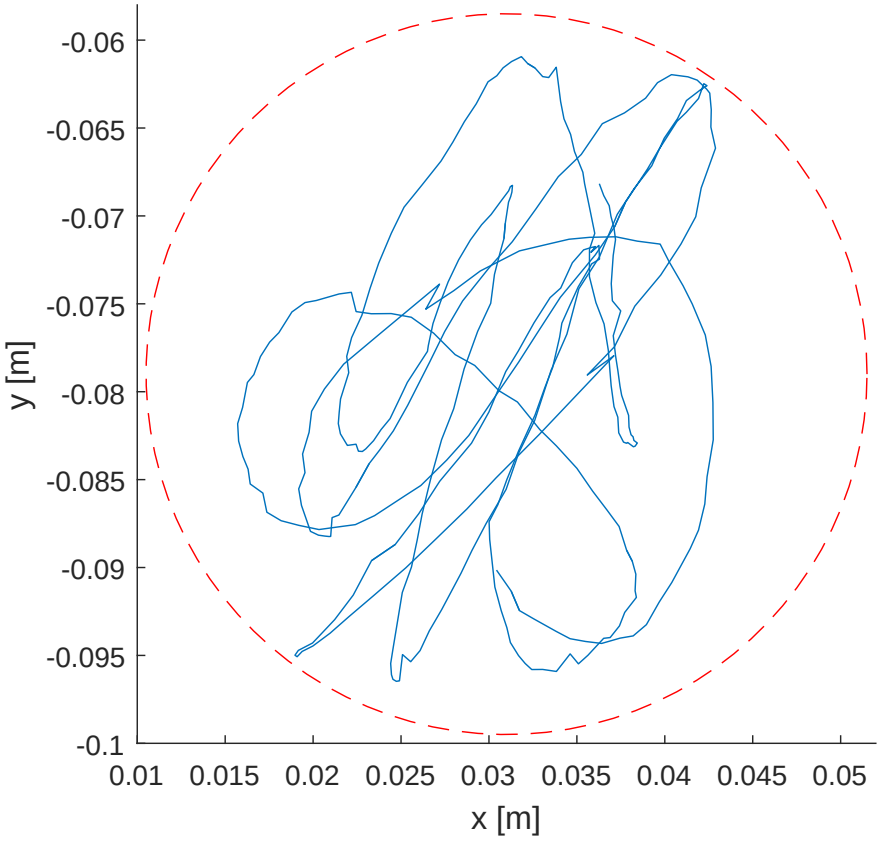

Figure 4.10: Vertical motion during altitude stabilization: quadcopter trajectory remains within a circular area with radius 2.05 *cm*.

4.4.3 Waypoint navigation

In this experiment waypoints were set up within the cage at the following (world) coordinates in meters:

- Waypoint 1: $WP1 = (-0.585, \ -0.030)$
- Waypoint 2: $WP2 = (0.020, \ 0.850)$
- Waypoint 3: $WP3 = (0.605, \ -0.030)$

The initial marker pivot location was close to the origin, at $(0.0174, \ -0.0329)$. The quadcopter must approach the waypoints within 1 *cm* in the same order as they were defined. These waypoints were pre-programmed into the control algorithm and the operator instructed the quadcopter to go to the next waypoint if the previous one has been reached. The camera

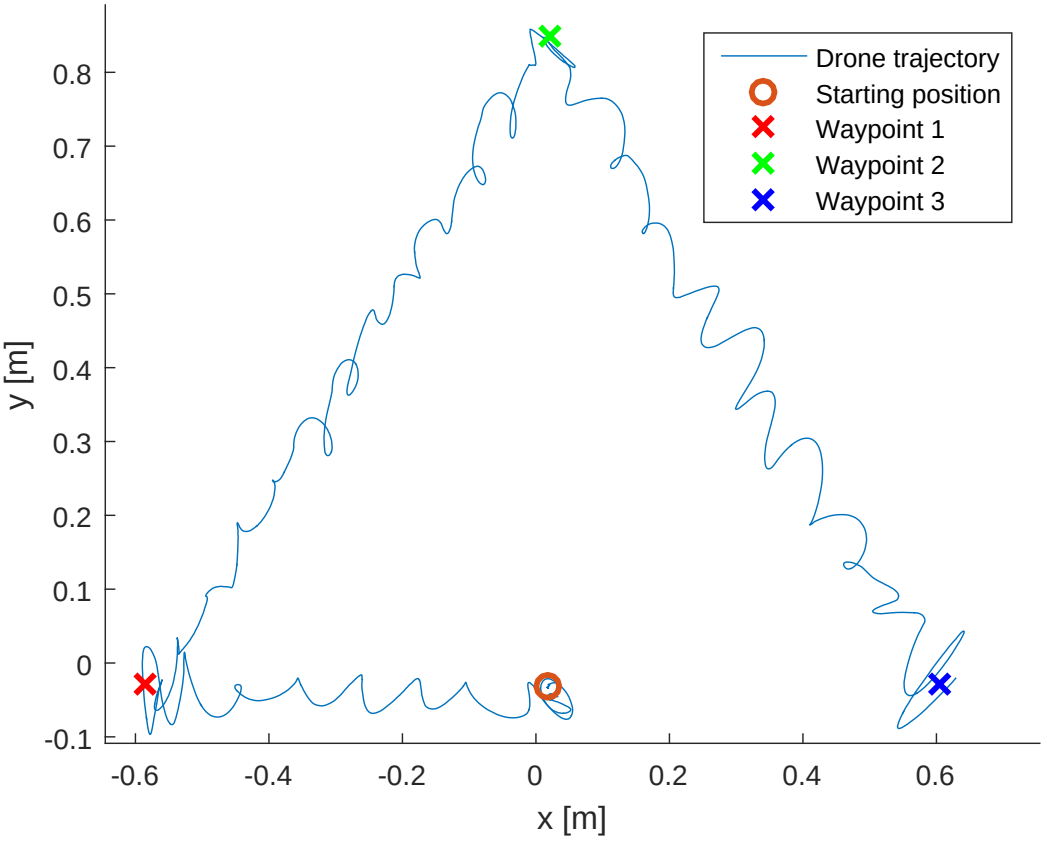

Figure 4.11: Quadcopter trajectory during waypoint navigation. The tolerance to consider a waypoint reached was set to 1 *cm*.

system is capable of measuring distance with sub-millimeter accuracy. The results can be seen in Fig. 4.11. The task was performed successfully, all waypoints were reached in order. The whole mission from take-off to landing takes around 75 *seconds*. The quadcopter trajectory is oscillating perpendicular to the heading direction, the amplitude of the oscillation is less than 6 *cm*.

Chapter 5

Conclusion and future work

This thesis aimed to introduce a new framework for the distributed control of leader- follower multi-agent systems with adjustable swarm control objectives. The mathematical model was employed to describe fundamental swarm behaviors such as aggregation and leader tracking.

In Chapter 2, aggregation and leader tracking problem was studied under a complete communication topology and under first-order and higher-order dynamics. Bounds on the swarm size and time of convergence have been derived.

However, in practical applications the agents' communication capabilities are limited, and therefore it is desirable to relax the assumption on the information exchange topology. In Chapter 3, the framework was extended to swarms where the interaction topology is described by an attraction and a repulsion graph with time-varying weights. Quantitative connection was established between the ultimate swarm size and the bounds on the time-varying weights under single-integrator agent dynamics. Extending these results to higher-order dynamics would constitute an essential step towards real-world implementation.

This study introduced a mathematical framework to model time-varying swarm objectives, but it does not discuss the question how to actually adjust the objective function in different situations. As a possible future study, it would be desirable to investigate transfer-of-control or autonomy-adjustment strategies, which would update the coupling weights based on some underlying algorithm. One direction would be the application of optimal control methods (based on cost function minimization) to find (sub)optimal weights in order to achieve the system level goal. An alternative approach is to develop adaptive control methods to update the weights based on some learning technique (for example neural networks).

Experimental validation is an important aspect of control systems engineering. Testing of a control framework is a challenging problem, which requires comprehensive knowledge of both the theoretical framework and the real-world system under control. In Chapter 4, first steps towards the experimental validation of the proposed distributed control scheme was demonstrated. PID control based position stabilization and waypoint navigation has been implemented for an *AscTec Hummingbird* quadcopter, where the position feedback was provided by a motion tracking camera system.

Although PID control design enables for fast design and testing even without deep understanding of the plant dynamics, it certainly has its limitations. Even though the designed controller showed satisfactory performance stabilizing the velocity in x and y directions, the coupling between roll, pitch and thrust cannot always be neglected as it was reflected by the issues with thrust control.

Therefore it is necessary in the future to identify the dynamic model of the quadcopter and design the controller based on that, where the velocity control in x, y, z directions is not decoupled. Better understanding of the plant dynamics and its uncertainties (both parameter and structural) would enable for more robust optimal control design such as H_2 or H_∞ control.

Moreover, the comparably large size of the used quadcopter model may constitute a serious problem in case the experiments are extended to several autonomous agents. It would be necessary to reproduce the same results for a robotic platform with smaller physical dimensions.

Another disadvantage of the *Hummingbird* is the lack of knowledge of the actual attitude control algorithm running on the onboard computer. The fact that only roll/pitch/yaw/thrust commands can be sent to the quadcopter (which will be tracked by a closed source controller) is also very limiting. Direct access to the DC motor voltages would enable for designing more advanced control algorithms.

Bibliography

[1] Asctec Hummingbird product overview. http://wiki.asctec.de/display/AR/AscTec+Hummingbird, . Accessed: 03/27/2017.

[2] P. Castillo, A. Dzul, and R. Lozano. Real-time stabilization and tracking of a four rotor mini-rotorcraft. pages 3123–3128, Sept 2003.

[3] CM Breder. Equations descriptive of fish schools and other animal aggregations. *Ecology*, 35(3):361–370, 1954.

[4] A. Okubo. Dynamical aspects of animal grouping: Swarms, schools, flocks, and herds. *Advances in Biophysics*, 22:1–94, 1986.

[5] J. Toner and Y. Tu. Flocks, herds, and schools: A quantitative theory of flocking. *Physical Review E*, 58:4828–4858, 1998.

[6] A. Colorni, M. Dorigo, and V. Maniezzo. Distributed optimization by ant colonies. *Proceedings First European Conference on Artificial Life*, pages 134–142, 1992.

[7] S. Das, A. Biswas, S. Dasgupta, and A. Abraham. Bacterial foraging optimization algorithm: Theoretical foundations, analysis, and applications. *Studies in Computational Intelligence*, 203:23–55, 2009.

[8] Dervis Karaboga. An idea based on honey bee swarm for numerical optimization. Technical report, Technical report-tr06, Erciyes university, Engineering Faculty, Computer Engineering Department, 2005.

[9] R. Olfati-Saber, J. A. Fax, and R. M. Murray. Consensus and cooperation in networked multi-agent systems. *Proceedings of the IEEE*, 95(1):215–233, 2007.

[10] R. Olfati-Saber. Flocking for multi-agent dynamic systems: algorithms and theory. *IEEE Transactions on Automatic Control*, 51(3):401–420, 2006.

[11] J. A. Fax and R. M. Murray. Information flow and cooperative control of vehicle formations. *IEEE Transactions on Automatic Control*, 49(9):1465–1476, 2004.

[12] J. Cortes, S. Martinez, T. Karatas, and F. Bullo. Coverage control for mobile sensing networks. *IEEE Transactions on Robotics and Automation*, 20(2):243–255, 2004.

[13] Veysel Gazi and Kevin M Passino. A class of attractions/repulsion functions for stable swarm aggregations. *International Journal of Control*, 77(18):1567–1579, 2004.

[14] J. Yao, R. Ordonez, and V. Gazi. Swarm tracking using artificial potentials and sliding mode control. *Journal of Dynamic Systems, Measurement, and Control*, 129:749–754, 2007.

[15] H. Yamaguchi. A cooperative hunting behavior by mobile robot troops. *Proceedings of the 1998 IEEE International Conference on Robotics and Automation*, 4:3204–3209, 1998.

[16] V. Gazi and K. M. Passino. Stability analysis of social foraging swarms. *IEEE Transactions on Systems, Man, and Cybernetics - Part B: Cybernetics*, 34:539–557, 2004.

[17] Hagen Schempf, Edward Mutschler, Colin Piepgras, J Warwick, Brian Chemel, Scott Boehmke, William Crowley, Robert Fuchs, and Joshua Guyot. Pandora: autonomous urban robotic reconnaissance system. In *Robotics and Automation, 1999. Proceedings. 1999 IEEE International Conference on*, volume 3, pages 2315–2321. IEEE, 1999.

[18] Štefan HavlÍk. A modular concept of the robotic vehicle for demining operations. *Autonomous Robots*, 18(3):253–262, 2005.

[19] Sebastian Thrun, Scott Thayer, Warren Whittaker, Christopher Baker, Wolfram Burgard, David Ferguson, Dirk Hähnel, Michael Montemerlo, Aaron Morris, Zachary Omohundro, et al. Autonomous exploration and mapping of abandoned mines. *Robotics & Automation Magazine, IEEE*, 11(4):79–91, 2004.

[20] Steven Scheding, Gamini Dissanayake, Eduardo Mario Nebot, and Hugh Durrant-Whyte. An experiment in autonomous navigation of an underground mining vehicle. *Robotics and Automation, IEEE Transactions on*, 15(1):85–95, 1999.

[21] Evan Ackerman. Amazon promises package delivery by drone: is it for real? *IEEE Spectrum, Web*, Dec. 2, 2013, Accessed: May 19, 2016.

[22] Peter R Wurman, Raffaello D'Andrea, and Mick Mountz. Coordinating hundreds of cooperative, autonomous vehicles in warehouses. *AI magazine*, 29(1):9, 2008.

[23] Phillip Walker, Saman Amirpour Amraii, Marlon Lewis, Nilanjan Chakraborty, and Katia Sycara. Human control of leader-based swarms. In *Systems, Man, and Cybernetics (SMC), 2013 IEEE International Conference on*, pages 2712–2717. IEEE, 2013.

[24] M. A. Goodrich, B. Pendleton, P. B. Sujit, and J. Pinto. Toward human interaction with bio-inspired robot teams. *Systems, Man, and Cybernetics (SMC), 2011 IEEE International Conference on*, pages 2859–2864, 2011.

[25] Ziyang Meng, Zongli Lin, and Wei Ren. Leader–follower swarm tracking for networked lagrange systems. *Systems & Control Letters*, 61(1):117–126, 2012.

[26] Hong Shi, Long Wang, and Tianguang Chu. Virtual leader approach to coordinated control of multiple mobile agents with asymmetric interactions. *Physica D: Nonlinear Phenomena*, 213(1):51–65, 2006.

[27] D. Gu. Leader follower flocking: Algorithms and experiments. *IEEE Transactions on Control Systems Technology*, 17:1211–1219, 2009.

[28] H. Su, X. Wang, and Z. Lin. Flocking of multi-agents with a virtual leader. *IEEE Transactions on Automatic Control*, 54:293–307, 2009.

[29] Raja Parasuraman, Thomas B Sheridan, and Christopher D Wickens. A model for types and levels of human interaction with automation. *Systems, Man and Cybernetics, Part A: Systems and Humans, IEEE Transactions on*, 30(3):286–297, 2000.

[30] Milind Tambe, Paul Scerri, and David V Pynadath. Adjustable autonomy for the real world. *Journal of Artificial Intelligence Research*, 17(1):171–228, 2002.

[31] B. Sellner, F. W. Heger, L. M. Hiatt, R. Simmons, and S. Singh. Coordinated multiagent teams and sliding autonomy for large-scale assembly. *Proceedings of the IEEE*, 94(7):1425–1444, 2006.

[32] J. W. Crandall and M. A. Goodrich. Experiments in adjustable autonomy. *IEEE International Conference on Systems, Man, and Cybernetics*, 3:1624–1629, 2001.

[33] Abdel-Illah Mouaddib, Shlomo Zilberstein, Aurélie Beynier, Laurent Jeanpierre, et al. A decision-theoretic approach to cooperative control and adjustable autonomy. In *ECAI*, pages 971–972, 2010.

[34] Paul Scerri, David V Pynadath, and Milind Tambe. Why the elf acted autonomously: Towards a theory of adjustable autonomy. In *Proceedings of the First International Joint Conference on Autonomous Agents and Multiagent Systems: part 2*, pages 857–864. ACM, 2002.

[35] Gregory Dorais, R Peter Bonasso, David Kortenkamp, Barney Pell, and Debra Schreckenghost. Adjustable autonomy for human-centered autonomous systems. In *Working notes of the Sixteenth International Joint Conference on Artificial Intelligence Workshop on Adjustable Autonomy Systems*, pages 16–35, 1999.

[36] P. Rani, N. Sarkar, and J. Adams. Anxiety-based affective communication for implicit human-machine interaction. *Advanced Engineering Informatics*, 21:323–334, 2007.

[37] C. Godsil and G. Royle. *Algebraic Graph Theory*. Springer, 2001.

[38] W. Li. Stability analysis of swarms with general topology. *IEEE Transactions on Systems, Man, and Cybernetics. Part B: Cybernetics*, 38:1084–1097, 2008.

[39] R. A. Horn and C.R. Johnson. *Matrix Analysis*. New York: Cambridge Univ. Press, 1985.

[40] B. Mohar. The laplacian spectrum of graphs. *Graph Theory, Combinatorics, and Applications*, 2:871–898, 1991.

[41] Y. Guan and G. Xu. Algebraic connectivity of weighted graphs under shifting components. *Discrete Mathematics, Algorithms and Applications*, 2:263–275, 2010.

[42] Z. Fabian and S. Y. Yoon. Coordination of multi-agent leader-follower system with time-varying objective function. *IEEE Conference on Decision and Control*, 2016.

[43] V. Gazi and K. M. Passino. *Swarm Stability and Optimization*. Springer, 2011.

[44] Veysel Gazi. Swarm aggregations using artificial potentials and sliding-mode control. *Robotics, IEEE Transactions on*, 21(6):1208–1214, 2005.

[45] H. K. Khalil. *Nonlinear Systems (3rd Edition)*. Prentice Hall, 2001.

[46] R. A. DeCarlo, S. H. Zak, and G. P. Matthews. Variable structure control of nonlinear multivariable systems: a tutorial. *Proceedings of the IEEE*, 76:212–232, 1988.

[47] Yanfei Liu and Kevin M Passino. Stable social foraging swarms in a noisy environment. *Automatic Control, IEEE Transactions on*, 49(1):30–44, 2004.

[48] Reza Olfati-Saber and Richard M Murray. Consensus problems in networks of agents with switching topology and time-delays. *Automatic Control, IEEE Transactions on*, 49(9): 1520–1533, 2004.

[49] Rodolphe Sepulchre, Derek A Paley, and Naomi Ehrich Leonard. Stabilization of planar collective motion with limited communication. *Automatic Control, IEEE Transactions on*, 53(3):706–719, 2008.

[50] Yoonsoo Kim and Mehran Mesbahi. On maximizing the second smallest eigenvalue of a state-dependent graph laplacian. *Automatic Control, IEEE Transactions on*, 51(1):116–120, 2006.

[51] Nair Maria Maia De Abreu. Old and new results on algebraic connectivity of graphs. *Linear algebra and its applications*, 423(1):53–73, 2007.

[52] Guixian Tian, Tingzhu Huang, and Shuyu Cui. Bounds on the algebraic connectivity of graphs. *Advances in Mathematics*, 41(2), 2012.

[53] M. Fiedler. Algebraic connectivity of graphs. *Czechoslovak Mathematical Journal*, 23: 298–305, 1973.

[54] Asctec onboard computer. http://wiki.asctec.de/display/AR/Onboard+Computer, . Accessed: 03/27/2017.

[55] Communicating with the Low Level Processor. http://wiki.asctec.de/display/AR/Communicating+with+the+Low+Level+Processor, . Accessed: 03/27/2017.

[56] Optitrack Flex 13 technical details. http://optitrack.com/products/flex-13/specs.html, . Accessed: 03/27/2017.

[57] Transform world-space coordinates to local rigid body coordinates. http://help.naturalpoint.com/kb/articles/transform-world-space-coordinates-to-local-rigid-body-coordinates, . Accessed: 03/27/2017.